Identifying Collisional Families in the Kuiper Belt

Robert A. Marcus[1,a], Darin Ragozzine[1], Ruth A. Murray-Clay[1], Matthew J. Holman[1]

[1]*Harvard-Smithsonian Center for Astrophysics, Cambridge, MA 02138*

[a]rmarcus@cfa.harvard.edu

ABSTRACT

The identification of numerous collisional families – clusters of bodies with a common collisional origin – in the asteroid belt has added greatly to the understanding of asteroid belt formation and evolution as well as physical processes that had previously been neglected (e.g., the Yarkovsky effect). Collisions have certainly played an important role in the evolution of the Kuiper belt as well, though only one collisional family has been identified in that region to date, around the dwarf planet Haumea. In this paper, we combine insights into collisional families from numerical simulations with the current observational constraints on the dynamical structure of the Kuiper belt to investigate the ideal sizes and locations for identifying collisional families, since Kuiper belt families do not generally form obvious tight clumps like asteroid families. We find that larger progenitors (∼500 km) result in more easily identifiable families, given the difficulty in identifying fragments of smaller progenitors in magnitude-limited surveys, despite their larger spread and less frequent occurrence. Where the background population has a well-known distribution in orbital elements, identifying families as statistical over-densities is much more likely, though less powerful, than characterizing families by distinguishing individual family members from interlopers in regions where the family outnumbers the background population. In either case, families will also be much easier to study where the background population is small, i.e., at high inclinations. Overall, our results indicate that entirely different family search techniques will be needed in the Kuiper belt and we provide some suggestions.

Subject headings:

1. Introduction

The Kuiper belt, the region extending beyond the orbit of Neptune, hosts a population of tens of thousands of small bodies larger than ∼100 km in diameter at distances mostly less

than ∼50 AU. Like the other major reservoir of small bodies in the solar system, the asteroid belt, the Kuiper belt has a complex structure that can be used to constrain theories of solar system formation. Kuiper belt objects (KBOs) can be divided into several distinct populations (e.g., Elliot et al. 2005; Gladman et al. 2008), with different histories, dynamics, and physical properties. A complete understanding of the varied properties of these populations requires constraints on the history of collisions among their members.

A number of collisional families – clusters of bodies originating from the break-up of a single parent body – have been identified in the asteroid belt (e.g., Parker et al. 2008). However, none were known to exist in the Kuiper belt prior to the discovery of a cluster of several bodies around the dwarf planet Haumea (provisional designation 2003 EL_{61}, Brown et al. 2007), the third largest known KBO (see Section 2.3). No other KBO families have been confirmed, and additional collisional families in the Kuiper belt are thought to be rare, or at least difficult to discover, for a number of reasons. Collisions typically result in a collection of objects with a velocity dispersion comparable to the parent body's escape velocity (e.g., Durda et al. 2007). Orbital velocities in the Kuiper belt are $v_{\rm kep} \lesssim 5$ km/s. With typical eccentricities in the classical belt of $e \lesssim 0.1$, relative velocities ($\sim ev_{\rm kep}$)between bodies are only hundreds of meters per second, less than the ∼1 km/s escape velocity of Pluto. Besides the fact that such low velocities would be insufficient to disrupt the largest (and most visible) bodies, the comparable size of the typical ejection velocity and the background velocity dispersion causes Kuiper belt families to spread across huge swaths of the trans-Neptunian region, significantly diluting the dynamical clumping of families that is so prominent in the asteroid belt.

The presence of the Haumea family suggests that many more families may be present at smaller sizes (Levison et al. 2008b). Chiang (2002) identified a dynamical clustering of bodies in the cold classical belt that at first glance appeared to be a family, but was later dismissed as a candidate family by Chiang et al. (2003) because of its very low velocity dispersion ($\sim$ 0.03 km/s) and concerns about the statistical significance of the clustering. We note here that the Haumea family also has an unusually low velocity dispersion and that perhaps the cluster identified by Chiang (2002) may represent the core of a larger collisional family that is harder to identify. Essentially the same region (with proper semi-major axis ∼44.2 AU, proper eccentricity of ∼0.07, and proper inclination of ∼2°) has also been identified by the CFEPS survey to have a statistically significant over-density and corresponds to their "kernel" region (Petit et al., submitted), which they also suggest may be a collisional family.

Though identification of collisional families in the Kuiper belt is difficult, the potential rewards are large. These groups provide a unique testbed for theories of the dynamical, collisional, interior, and surface properties of KBOs. If found, further KBO families will

provide valuable insights into properties of individual objects and the outer solar system as a whole that are otherwise difficult to obtain. In this paper, we emphasize the constraints on Kuiper belt formation and evolution that can be inferred from the presence or absence of families with varying properties in the belt. We mention two other specific examples of science that can be done with KBO families here.

First, the expected size-frequency distribution of a collisional family depends on physical characteristics of the impactors, and this distribution can be modeled by smoothed particle hydrodynamics (SPH) simulations. Such simulations have been performed for the asteroid belt (Durda et al. 2007). However, in the asteroid belt, the size-velocity distribution of a family cannot be well constrained because of the Yarkovsky effect—a thermal radiation force that causes small bodies to undergo semi-major axis drift as a function of their spin, orbit, and material properties (Bottke et al. 2002). In the Kuiper belt the Yarkovsky effect is minimal (see Section 3.3), and many of the details of the velocity distribution and the ejection field can be determined quite well *if* there are a large number of family members that can be distinguished from interlopers. Improving our understanding of collisions between these icy bodies is directly connected to the formation of outer solar system planets, since planetesimals beyond the snow line including, presumably, giant planet cores were formed by collisions between icy bodies.

The second example of unique science that can be addressed with collisional families relates to the surface properties of KBOs. KBO surfaces, as probed spectrally or by color observations, present few trends, and there is no clear over-arching theory that explains the observations. It is not yet clear whether a KBO's color is determined by its composition, as suggested, e.g., by Benecchi et al. (2009), or by its current orbital environment, as could be inferred from Sheppard (2010), or some combination of the two. Collisional families provide a useful touchstone for KBO colors since it can be reasonably assumed that most of the fragments are of similar composition, giving insight into the "nature vs. nurture" element of KBO colors. Another aspect of surface physics that can be probed by families is space weathering. Surprisingly, the Haumea family is known to be dynamically old (Ragozzine & Brown 2007; Levison et al. 2008b) but the surfaces appear in all respects to be fresh and recently resurfaced (Rabinowitz et al. 2008; Elliot et al. 2010). Recent work on very young asteroid families has been able to give constraints on the rate and type of space weathering (Vernazza et al. 2009). We suspect that finding additional KBO families will clarify the nature of KBO surfaces, especially given the precision color photometry expected from the next generation of all-sky surveys like Pan-STARRS and LSST.

Given the likely difficulties in identifying collisional families in the Kuiper belt, we need to understand the orbital and size distributions of the background population, and how

these would be modified by family-forming collisions. The Kuiper belt is divided into three distinct regions, which we review here. The first of these is the classical belt, consisting of a cold population at low inclination and a dynamically excited (hot) population at inclinations larger than $\sim 5^\circ$. Besides evidence for these two populations in the inclination distribution (Brown 2001), they are also apparently distinct in eccentricity (Kavelaars et al. 2009), color (Peixinho et al. 2008), sizes (Levison & Stern 2001), albedos (Brucker et al. 2009), binary fraction (Noll et al. 2008), and size distribution (Fraser et al. 2010). A second population is inherently unstable on ∼Gyr timescales and are known as scattering/scattered disk objects, since they are in orbits that are scattering off of Neptune, usually with perihelia below ∼35-40 AU. The third population are "resonant" KBOs, bodies in mean-motion resonance with Neptune, and can be divided into two sub-categories: "push-out resonants" which are deep within resonances with typically low resonant libration amplitudes and which appear to have been pushed out by the migration of Neptune (e.g., Malhotra 1995) and "sticky resonants" which are scattered disk objects that have been temporarily captured in resonance (e.g., Lykawka & Mukai 2007). The size distribution of KBOs seems to vary between populations, at least above a diameter $\sim$ 100 km (Fuentes et al. 2010), at which there is a break likely due to the collisional erosion of bodies smaller than this size (Bernstein et al. 2004; Pan & Sari 2005). The total mass of the Kuiper belt is $0.01 - 0.1 M_\oplus$, but not larger than $0.25 M_\oplus$, considerably larger than that of the asteroid belt ($\sim 0.0004 M_\oplus$) (Kavelaars et al. 2009; Pitjeva 2010). All of these populations in the trans-Neptunian region have experienced collisions, either with objects from the same population or with objects from the other overlapping populations, and collisions continue to this day, at least among small objects.

In this paper, we investigate the likelihood of identifying collisional families in the Kuiper belt with parent bodies of intermediate sizes in the range 100-500 km, where much of the mass in the Kuiper belt is currently located. The expected velocity dispersion for such families, $\sim 100 - 300$ m/s is smaller than the typical background velocity dispersion of ∼1 km/s, while many of the family members are still likely to be observable with upcoming surveys (e.g., Pan-STARRS, LSST). In Section 2 we discuss the properties of known collisional families and we combine this with models for the formation and evolution of the Kuiper belt in Section 3 to estimate what types of families we expect to exist in the Kuiper belt. In Section 4 we discuss our method of generating a synthetic background and synthetic families and in Section 5, we present our results of these simulations and the some insights gained therefrom. Finally, in Section 6, we discuss their implications for finding additional collisional families in the Kuiper belt.

2. Background on Collisional Families

A collisional family is a set of objects that were originally part of the same parent body. In this section, after introducing the concept of proper elements (Section 2.1), we discuss asteroid belt collisional families (Section 2.2), and the Haumea collisional family (Section 2.3). We then describe expectations for any additional KBO families (Section 3).

2.1. Proper Elements

Families are identified by linking a set of objects that likely originated from very similar heliocentric positions and velocities and thus had nearly the same (osculating) heliocentric orbital elements at some point in the past. Some differences in the osculating elements between family members are expected because the collision that forms the family gives each member an independent velocity kick relative to the center-of-mass orbit of the two colliding bodies. The initial collision does not generally change the orbital angles – ω, the argument of periapse, Ω, the longitude of the ascending node, and M, the mean anomaly — by more than $\sim 10^\circ$, depending on the velocity of impact and the orbit. Over time, since each family member has a slightly different semi-major axis, they have different periods and the orbital phase (given by the mean anomaly) is randomized after several orbital periods (which is why families are not clustered in their present-day locations in the sky). On secular timescales, the differing semi-major axes impart to each family member a slightly different apsidal and nodal precession rate, causing the orbital angles ω and Ω to also randomize. The information in these angles — that all of the family members had similar values — is lost.

For objects which are on stable orbits, the so-called "proper" or free orbital elements, e_{proper} and i_{proper}, are roughly conserved in secular theory, along with the osculating semi-major axis, a. Proper elements are time-conserved quantities that describe the orbital characteristics and are calculated by removing the time-dependent perturbations by the major planets. The value of the proper elements depends on the positions of the planets and all the orbital elements; however, since the original family started at the same time, with somewhat similar orbital elements, they have a similar spread in proper orbital elements as in the initial osculating elements. Thus, groups of objects with similar proper elements may have shared very similar orbits in the past, potentially due to a common origin in a particular collision. Current observations of KBOs allow for a quite accurate measurement of proper orbital elements; in general, clustering in these orbital elements will not be hindered by observational uncertainty. Hence, the search for collisional families focuses on finding clusters among proper element distributions of stable objects.

In this paper, we focus on families produced in the classical region of the Kuiper belt. The scattered disk region and the Centaur region, which are both dynamically unstable, are unlikely to harbor observable collisional families, unless these families are very young ($\lesssim$10 Myr) and not yet dispersed dynamically. Long-term families could, however, exist in stable mean motion resonances with Neptune. Resonant KBOs also have conserved quantities (the proper libration amplitude, proper eccentricity, and proper inclination, for example) and multiple asteroid families have been identified in resonances with Jupiter (e.g., Brož & Vokrouhlický 2008), particularly the 1:1 resonance inhabited by Trojans (Milani 1993). Objects in resonances, especially weaker resonances, are likely to undergo some weak chaos (Nesvorný & Roig 2001), but Ragozzine & Brown (2007) point out that even these objects can still have more-or-less conserved proper semi-major axes and proper Tisserand parameter. The existence or absence of resonant families, particularly among the Neptune trojans, would be very interesting. However, only the smallest families will "fit" inside Neptune resonances; even the large 3:2 resonance can be easily escaped by Plutinos with ejection velocities as low as 20 m/s, implying that the progenitors of such families would need to be $\sim$20 km in size, making such families extremely difficult to observe due to the faintness of family members (see also, Hahn & Ward 1995).

Larger, more visible families, can easily cover several resonances and presumably emplace objects in these resonances as seen in the case of Haumea's collisional family (Ragozzine & Brown 2007). Furthermore, some of these resonances create weak chaos with timescales comparable to the age of the family, allowing chaotic chronology (e.g., Milani & Farinella 1994; Ragozzine & Brown 2007) to be used as a method for determining an absolute age, albeit without much precision, as in the case of the Haumea family and its age of 3.5 ± 2 Gyr (Ragozzine & Brown 2007). Collisions between small bodies and the subsequent dispersal of objects implies that the orbital distribution of sub-populations (like the cold classicals) could change as a function of size. Furthermore, we note with Davis & Farinella (1996) that the frequent collisions between very small bodies and emplacement of fragments into unstable resonances could play an important role in the delivery of comets to the inner solar system.

2.2. Asteroid belt collisional families

Hirayama (1918) first identified clusters of main belt asteroids that were likely of a common origin. Roughly half of all known asteroids are in identified families (Zappala et al. 1995). Such families are now known to have formed from collisions between asteroids. Asteroid collisional families are identified dynamically by clustering in proper orbital elements and spectroscopically by the distinct color differences between different families and between

family members and background objects.

While rough calculations of the proper orbital elements can be carried out analytically, as was done by Hirayama (1918), these analytic expressions are only valid to first order, and accurate family member identification of asteroids today requires numerical orbit integration coupled to frequency filtering of the periodic perturbations from the planets (e.g., Knežević & Milani 2000). Likewise, identification of family members has advanced beyond visual inspection of proper eccentricity and proper inclination versus semi-major axis plots to include clustering algorithms, with a metric given by, e.g.

$$\partial v = na' \sqrt{5/4(\delta a'/a')^2 + 2(\delta e')^2 + 2(\delta \sin i')^2} \quad (1)$$

with the coefficients fine-tuned to produce accurate results (Zappala et al. 1990). Here ∂v is a distance in proper element space with dimensions of velocity, while n, a', e', i', are the proper mean motion, semi-major axis, eccentricity, and inclination of the particles, respectively. Note that the commonly employed Hierarchical Clustering Method, which links family members together through a friends-of-friends technique, assumes that the family is tightly clumped relative to the background, a criterion that is not always satisfied in the Kuiper belt, as will be shown in Section 5.

Using these techniques, at least 20 asteroid families have been identified, although the ratio of family members to non-family members at small sizes is still unclear (Cellino & Dell'Oro 2010). The identification of families has led to detailed numerical studies of the collisional processes that form families. The results of numerical simulations show that asteroid collisional families have formed both by catastrophic disruption of a parent body and by cratering impacts (e.g., Durda et al. 2007).

2.3. Formation of the Haumea Collisional Family

The Haumea family was initially identified by the discovery of a class of objects with unusually deep water ice spectra, and was later shown to be tightly clustered dynamically, with a velocity dispersion of only $\sim$ 140m/s (Brown et al. 2007; Barkume et al. 2008; Ragozzine & Brown 2007), much smaller than the escape velocity from Haumea ($\sim$ 900m/s). Brown et al. (2007) proposed a collisional origin for the family members, with a high velocity ($\sim$ 3 km/s) impact stripping the proto-Haumea (with an initial density of 2.0 g/cm^3, consistent with other large KBOs) of some of its icy mantle and leaving behind the $\sim$2.6 g/cm^3, rapidly rotating dwarf planet, along with its two satellites and associated family members.

A collisional scenario like that proposed by Brown et al. (2007) is only probable early in the solar system in the thin pre-excitation planetesimal disk, but subsequent scattering

by Neptune into the current Kuiper belt would have destroyed the dynamical coherence of the family. Levison et al. (2008b) proposed a collisional scenario in which two scattered disk objects collided after the Kuiper belt was already excited and resulting in the formation of the Haumea family in the excited classical region. Such a scenario renders plausible a collision between two large KBOs and preserves the dynamical coherence of the family, but it does not explain the low velocity dispersion between family members. Schlichting & Sari (2009) later proposed a scenario in which a giant impact creates a rapidly-rotating, high-density Haumea with a large satellite. A subsequent impact onto the satellite (after Haumea is on its current orbit) forms the family with a low velocity dispersion in an order-of-magnitude sense. However, detailed numerical simulations of the collisional scenarios of Brown et al. (2007) and Schlichting & Sari (2009) show that such collisions are unlikely to explain the near-breakup spin rate of Haumea (Leinhardt et al. 2010). Instead, Leinhardt et al. (2010) suggest a scenario in which the family formed directly by a single low-speed "graze and merge" impact event, as also recommended by Toth & Lisse (2010). This impact event is able to explain the low velocity dispersion of the family, the presence of both satellites and unbound family members, and the near-breakup rotation and enhanced density (relative to other large KBOs) of Haumea. It is still unclear, however, how such an impact scenario would arise, as any collision with Haumea in the current Kuiper belt environment would be a high-speed event.

Ragozzine & Brown (in prep) suggest a graze and merge collision caused by disruption of a large proto-binary, which can qualitatively satisfy all the constraints, but which has not been investigated in detail. Though the precise formation mechanism for the Haumea family remains uncertain, the presence of one large KBO family highly suggests that there should be many smaller families. We should not assume that these smaller families will have similarly unique characteristics; for the families discussed in this paper, we generally adopt the more "typical" outcome of an ejection velocity similar to the escape velocity from the largest fragment (Leinhardt & Steward, in prep.). It is important to note that the Haumea family members have unusually high albedos (Elliot et al. 2010), suggesting that additional families will require deeper surveys to detect.

3. Expectations for KBO Families

Before discussing the observability of KBO families, we outline here expectations for what families may exist and remain coherent in the Kuiper belt, by drawing on the large amount of research on asteroid families and various theories for the formation and evolution of the Kuiper belt. After reviewing the details of collision physics that informs how families

formed (Section 3.1), we consider the implications of outer solar system formation models on when KBO families formed (Section 3.2). In Section 3.3, we describe the application recent results in asteroid family research on young families, asteroid pairs, Yarkovsky, and YORP in the Kuiper belt.

3.1. How Did Families Form?

The asteroid belt includes identified collisional families that have formed by cratering impacts as well as those formed by catastrophic disruption (e.g., Durda et al. 2007). A major (and obvious) feature of those families formed in cratering events is that the largest impact fragment is considerably smaller in size than the target body. This size difference can be an order of magnitude in radius or larger (i.e. ∼5 magnitudes fainter), with a smooth concave size-frequency distribution between the largest fragment and the smallest resolved fragments. While such family-forming collisions likely occur in the Kuiper belt, these are not the most likely families to be found, particularly around parent bodies of radius $\lesssim$ 500 km, due to the extreme faintness of nearly all the family members. Similarly, super-catastrophic impacts are also unlikely to result in identifiable families in the Kuiper belt because all of the fragments would be considerably smaller than the parent body.

Catastrophic collisions, in which the target body is entirely broken up, but roughly half the mass re-accretes due to gravity, are then the most likely source of any asteroid belt family analogs that will be identifiable in the Kuiper belt. In such collisions, roughly half the total colliding mass ends in the largest fragment. The differential size distribution of the remaining fragments is well-described by a power-law, $N(\geq r) \propto r^{1-q}$, with index $q \approx$4-5.5, that conserves the total mass and geometric volume prior to the collision and cuts off at some non-zero minimum size (Leinhardt & Stewart, in prep). The velocity distribution of the fragments spans the range with some velocities larger than the escape velocity and some smaller than the escape velocity with respect to the largest remnant (Leinhardt & Stewart, in prep), with a significant number (of order 10%) of the fragments having a velocity $\lesssim v_{\rm esc}$.

The type of impact necessary for catastrophic disruption of a parent body can be calculated using the catastrophic disruption criteria of Stewart & Leinhardt (2009), where the catastrophic disruption threshold is given by (in cgs units):

$$Q^*_{RD} = 10^{-4} R_{C1}^{1.2} V_i^{0.8}, \tag{2}$$

combined with the universal law for the largest remnant mass (M_{lr}):

$$M_{lr}/M_{tot} = -0.5(Q_R/Q^*_{RD} - 1) + 0.5\,. \tag{3}$$

Here R_{C1} is the radius of a spherical body containing the entire colliding mass (M_{tot}) at a density of 1 g cm^{-3}; V_i is the impact velocity; and $Q_R = \frac{1}{2}\mu V_i^2/M_{tot}$ is the reduced mass kinetic energy, scaled to the total colliding mass. Half the mass remains in the largest remnant when $Q_R/Q^*_{RD} = 1$. At typical relative velocities in the cold classical belt of $ev_{\rm orb} \approx 0.1 \times 5$ km/s $\approx$ 500m/s, catastrophic disruption is very unlikely to occur for target bodies larger than $\sim$ 100 km in radius. However, at the higher inclinations and eccentricities of the dynamically excited classical belt, typical relative velocities of $v_{\rm imp} \approx \sqrt{e^2 + i^2}v_{\rm orb} \approx \sqrt{0.1^2 + 0.3^2}v_{\rm orb} \approx 1.6$ km/s can lead to impacts that disrupt even 500 km target bodies.

The probability, p, of a collision between two bodies of sizes R_i and R_t in a time t_l is (Levison et al. 2008b)

$$p = N_i N_t t_l (R_i + R_t)^2 \bar{\rho}, \tag{4}$$

where N is the number of objects and $\bar{\rho}$ is the mean intrinsic impact rate. Adopting the value $\bar{\rho} = 1.7 \times 10^{-22}$ km^{-2} yr^{-1} as a reasonable mean impact rate for the entire Kuiper belt assuming it has always existed as it is today (as in Levison et al. 2008b), the probability of a collision between a 500 km target and a 350 km projectile in the age of the solar system is $\sim 4 \times 10^{-3}$. The probability reaches ~ 1 for a single collision between a 250 km target and a 100 km projectile since the Kuiper belt attained its current form. Note that these projectile sizes are chosen as the smallest objects that could catastrophically disrupt the target body at typical impact velocities $V_i = \sqrt{v_{\rm rel}^2 + v_{\rm esc}^2}$. While $\bar{\rho}$ is an average for the entire classical belt, we do not expect this to vary much between the subpopulations because the mean intrinsic impact rate is proportional to the velocity dispersion divided by the volume; the ratio of the volumes of the hot and cold populations is the same as the ratio of their scale heights (velocity dispersions), thus $\bar{\rho}$ is roughly the same for both. Without performing the detailed calculations done by Levison et al. (2008b), one would expect $\bar{\rho} \approx v_{disp}/V \approx \Omega/(\pi a^2) \approx 2 \times 10^{-22}$ km^{2}yr^{-1}, very close to the calculated value. Note that these probabilities may be increased by considering enhancements of the Kuiper belt populations in the past as discussed in Section 3.2.

Because of the steep slope in the size distribution for KBOs, collision probabilities significantly increase with decreasing size of the target and projectile; families are more likely to exist around smaller parent bodies. In addition, the differential size distribution of collisional families has a steeper slope, q≈4-5.5 (Leinhardt & Stewart, in prep), than the background population below the break in the size distribution, where q≈1.5-2.5 (Fuentes et al. 2009; Fraser & Kavelaars 2009). From these two facts, one would conclude that collisional families are more likely to be found as the largest remnants of smaller parent bodies, a topic that we will return to in Section 6 with more information.

3.2. When Did KBO Families Form?

Following Levison et al. (2008b), there are three major stages in the history of the Kuiper belt as found in virtually all successful models of the formation and evolution of the outer solar system (see e.g., recent reviews by Chiang et al. 2007; Levison et al. 2008a; Morbidelli et al. 2008). In Stage I, KBOs were in an environment where they could grow, which implies a large quiescent planetesimal disk where collisions were common, but gentle and leading to accretion (Kenyon et al. 2008). A dense thin planetesimal disk is also required for the formation of observed KBO binaries (Schlichting & Sari 2008). The Kuiper belt that we see today is neither massive nor dynamically quiescent: 100-1000 times more mass is needed to grow the observed objects. Thus, there must have been some sort of dynamical event (Stage II) that significantly excited the orbits of the KBOs. This event was either violent enough to perturb ∼99% of the primordial objects onto planet-crossing orbits, thereby dynamically producing the Kuiper belt's small mass, or excited the Kuiper belt enough that collisions became erosional, removing the extra mass by pulverizing objects to dust, r some combination of the two. It was during this violent period that most of the structure of the observed Kuiper belt was established. Since this dramatic event, the Kuiper belt has been relatively quiet (Stage III). The only significant dynamical changes may have resulted from the continuing collisions among the smaller bodies and the gradual decay of intrinsically unstable populations. This stage corresponds to the last ∼4 billion years of solar system history.

Collisions in the Stage I planetesimal disk may have produced families, but the subsequent excitation of the disk removes all signatures of these families (no orbital properties are conserved) and they cannot be studied at the present day. Only towards the end of Stage II, when the remaining dynamical evolution of Neptune is small, can one hope to conserve orbital properties that are observable today (though Levison et al. (2008b) do find that smooth low-eccentricity Neptune migration is not efficient at capturing Haumea-family members and that the shape of this family would be preserved). These "primordial" families are particularly valuable probes of Kuiper belt formation, since they were created in an environment that cannot be observed today, but which varies between different outer solar system formation models. For example, if the age of a currently coherent collision family in the excited population (perhaps the Haumea family) could be securely measured to be more than ∼4.1 Gyr ago, then a connection between the formation of the Kuiper belt and the late heavy bombardment ($\sim 3.8 - 4.1$Gyr ago), as proposed by the Nice model, could potentially be ruled out (Gomes et al. 2005).

During Stage II, the mass of the Kuiper belt is being eroded and the dynamical sculpting of the currently observed KBO orbits is accomplished. Depending on how these two,

potentially separate, processes were completed affects where we would find KBO families today. If objects were on their final orbits before most of the mass was removed by collisional grinding, then the frequency of families will be high, since the appropriate number density to assume for collision probabilities is much higher than seen today. On the other hand, if mass was removed dynamically, then there would presumably be a somewhat enhanced number of collisional families only after orbits have mostly settled down, so that the number of coherent families to observe today would be much less.

This concept has a specific application to the Kuiper belt in the as yet unclear origin of the cold classical population. One model proposes an *in situ* formation, with collisional grinding doing most of the work of removing mass from this region, while another, inspired by the Nice model, proposes that Neptune scattered with large eccentricity to an orbit near its current location, and the cold classical population was emplaced as Neptune's eccentricity damped (Levison et al. 2008a).

We can estimate the differences in the number of families produced by these two models. When the cold classical population forms in situ, the beginning of Stage III comes after the dynamical perturbation that imparted the observed eccentricities and inclinations to the pre-excitation planetesimal disk that initially extended to ∼45 AU. It is this early part of Stage III that creates the most families that remain coherent to the present day. For this case, assuming that dynamical perturbation removed 50% of the original mass, the collisional cascade starts with basically the observed cold classical belt with 50-500 times as many objects as are currently present (Kenyon et al. 2008). The size distribution would not necessarily be the same as observed today and one could expect, following Pan & Sari (2005), that it was mostly objects below the currently observed break that participated in the collisional cascade (Kenyon et al. 2008). This significantly increases the number of impactors, though, as in Levison et al. (2008b), we should account for the fall-off of this number enhancement as a function of time. We estimate that this leads to an increase in the number of families in the cold classical belt by a factor of 5-100 times over what would be predicted based on the currently observed belt. How this factor is calculated as a function of the size of the progenitor and whether we expect an enhancement of families at sizes larger than the ∼50 km break in the size distribution, depends on the detailed collisional grinding history. The size of the largest progenitor to have received a catastrophic collision in the age of the solar system may increase.

On the other hand, in a model (like that Nice model) that predicts dynamical emplacement of the cold classical population, the number of expected families is far fewer. In this formation scenario, the Stage I pre-excitation planetesimal disk extends to only ∼30 AU, and a major instability among the giant planets puts Neptune on an eccentric orbit. While

Neptune's orbit is eccentric, the cold classical region is dynamically unstable, allowing objects scattering off Neptune to fill this region. Though there are collisional families formed in the cold classical region during this time, they can not remain dynamically coherent until Neptune's orbit circularizes. At this point, formerly unstable objects in the cold classical region are stranded in the stable orbits observed today. In this model, the cold classical population starts out much smaller than in the in situ formation model. Though this population can decrease over time due to weak chaos, the decrease is not significant (particularly given the uncertainties in the size of the cold classical population as constrained by observations). Thus, a Nice-model-like emplacement of the cold classical population would have far fewer families than in the collisional grinding model.

Though families are certainly not the only way of elucidating which model or combination of models represents the actual history of the solar system, the purpose of this discussion is to highlight how the frequency of families (especially as a function of orbital properties and time) is a sensitive tracer of an otherwise model-dependent collision history. We note that Kuiper belt families can provide a unique window into the early outer solar system because the families are preserved for billions of years, unlike asteroid families, which formed almost exclusively in the past billion years.

Whichever the formation model, families continue to form throughout Stage III. These formation events can involve collisions between objects in stable and/or unstable populations. Unstable populations, such as the scattered disk, must have been much larger in the past, significantly increasing the number of collisions expected in the early outer solar system, as discussed in detail by Levison et al. (2008b). The scattered disk population must have been 100 times bigger in the past, with a relatively rapid decay constant, leading to an increase in the number of expected families by a factor of $\sim$25, which is needed to increase the probability of a putative Haumea collision.

Not all of these collisions produce families that are dynamically stable. Levison et al. (2008b) looked at the "collision orbits" of combinations of impactors in three model scattered disk populations assuming a fixed mass ratio of 5 between impactor and target and found that 10-30% of such collisions would emplace families in the stable region of the Kuiper belt, mostly with high perihelia and a large range of inclinations (see their Figure 2). The results would be different for different assumed mass ratios, i.e. as the mass ratio approaches infinity, the collisions do not change the orbit of the target, so all families would remain in the scattered disk and 0% would be emplaced in the Kuiper belt. It is beyond the scope of this paper to reassess their model for different mass ratios, but a mass ratio of 5 is generally reasonable, and we adopt the result that roughly 10-30% of SDO-SDO families are emplaced in the Kuiper belt, where they are stable and observable today. This leads to an increase

in the number of families by about a factor of ∼2-8, over what would be assumed based on the currently observed population. The size of the largest progenitor family thus created is that due to the Haumea family, presumably, and the next largest would be ∼400 km. We note that the tendency of such families to have high perihelia combined with the large spread created by Kuiper belt families means that family searches should look for truncated families which straddle the boundary between the stable Kuiper belt and the scattered disk.

Stage III families from stable populations are more rare, but do happen, even to the present day. As the number of KBOs in all populations is decreasing as a function of time, while the formation of large families leave a permanent mark (in dynamically stable regions), one would expect that typical KBO collisional families are very old. Families that are small enough such that the family members have collisional lifetimes significantly shorter than the age of the solar system, i.e., below the break in the size distribution at ∼ 50 km (Pan & Sari 2005) radius, will undergo secondary collisions that may effectively erase the original family in favor of creating many smaller newer families. Just how this process plays out will depend on the particular family in question and will need to be tested by observations. In general, relatively recent collisions can be identified as "young" families.

3.3. Young Families, KBO Pairs, Yarkovsky, and YORP

In some size range, collisions between Kuiper belt objects happen regularly and thus there are so-called "young" families that have formed recently. In the asteroid belt, "young" families are those for which the apses and nodes have not yet randomized or which are still tightly connected Nesvorný et al. (2002). We expect the Kuiper belt to also have young families, though due to the lower precession rates, the clustering in apses and nodes can last much longer (∼100 Myr or longer). Based on the collision rate described above, we estimate the radii at which a single KBO is likely to have undergone a catastrophic collision in the last 1, 10, and 100 Myr as 50 km, 70 km, and 100 km, respectively, with the currently observable collisional fragments a few times smaller. At the typical distance of 42 AU the brightness of such objects would be about 24.8 ,24.2, and 23.4 V magnitudes, respectively. Assuming half the mass of the progenitor is retained in the largest remnant, this remnant has a radius $0.5^{1/3}$ that of the progenitor and thus is fainter by $2.5 \log 0.5^{2/3} \approx 0.5$ magnitudes. Identifying the next N fragments from a collision requires observing $\frac{5 \log(N)}{q-1}$ magnitudes deeper than the largest remnant. This implies that young families will be observable in the Kuiper belt if it is surveyed down to $m_v \approx 26$, which is possible with LSST using shift-and-stack KBO detection methods.

Many known KBO binaries are very weakly bound and are thought to be susceptible to

disruption by passing KBOs, as discussed by Petit & Mousis (2004), though some of their adopted parameters of the Kuiper belt are somewhat out of date. If binaries are or were susceptible to disruption, the result is two KBOs with very similar heliocentric positions and velocities. Recently separated asteroid pairs have been discovered by Vokrouhlický & Nesvorný (2008), who show that using a separation metric that depends on all orbital elements, including mean anomaly, results in a significant excess of objects at small separation. In one case, a backwards integration shows that two asteroids were bound about 17000 years ago (Vokrouhlický & Nesvorný 2009).

Clustering in all orbital elements, including mean anomaly, requires a very recent separation, since this angle randomizes very quickly. Assuming that the velocity separation at infinity for these unbound binaries is comparable to the orbital velocity near the Hill sphere (the Hill velocity) and that this velocity is applied completely to a change in semi-major axis, the mean anomalies of KBO pairs would be randomized in $\gtrsim 10^6$ years. While it is thought that asteroid binaries may be constantly created by fission (Pravec et al. 2010), KBO binaries are primordial. Any process that would separate a binary in the last Myr would have been much more probable earlier in the history of the solar system, for multiple reasons. Thus, typical dissolved KBO binaries are not likely to be recent and would not have similar mean anomalies, though these may still be identified as objects with unusually similar orbits.

The Yarkovsky and YORP (Yarkovsky-O'Keefe-Radzievskii-Paddack) effects couple the thermal properties of asteroid surfaces with their heliocentric orbits and have been clearly observed in the asteroid belt, especially in association with asteroid families (see, e.g., review by Bottke et al. 2006). Though the solar flux in the Kuiper belt is hundreds of times smaller than in the asteroid belt, the gravitational pull of the Sun is correspondingly also hundreds of times weaker. The Yarkovsky and even YORP effects should be present in the Kuiper belt, so we mention them briefly here. We note that the importance of the Yarkovsky effect in the Kuiper belt has been discussed in an unpublished manuscript by D. Majaess & J. Hahn [1]. They find that the diurnal Yarkovsky effect is negligible for Kuiper belt objects with typical rotational periods; this was also the conclusion of Bottke et al. (2006). Similarly, the YORP effect on spin rate and obliquity is negligible at the distance of the Kuiper belt in the size range of interest here.

The seasonal Yarkovsky effect can have some effect in the Kuiper belt. Using the derivation of Vokrouhlický (1999), and assuming reasonable values for the thermal properties of Kuiper belt objects, Majaess & Hahn find that ∼30-meter bodies have the maximal

[1] http://www.ap.smu.ca/∼smuaps/thesis/Thesis-DJM-2005.pdf

possible drift, with rates approaching ∼1 AU/Gyr, where various assumptions make these values uncertain by at least an order of magnitude. Larger objects drift slower, with $\dot{a} \approx 1(\frac{r}{30\text{ m}})$ AU/Gyr. For the smallest objects we are considering, with a radius of 5 km, the maximal expected drift is ∼0.02 AU over the age of the solar system, which is negligible for understanding these bodies, as is the expected change in other orbital elements due to Yarkovsky. For smaller objects that have become Jupiter family comets or are observed by stellar occultations (e.g., Schlichting et al. 2009), the Yarkovsky effect on KBOs is more important.

4. Method

Our goal is to inject synthetic families into a synthetic KBO population to investigate directly how the expected families described above will appear, to make quantitative estimates of family detectability, and to provide insight into possible KBO family finding algorithms.

To estimate the background population of KBOs, we obtained the Pre+L3 Model synthetic Kuiper belt object population of the Canada-France Ecliptic Plane Survey (CFEPS) (Kavelaars et al. 2009). [2] This population is a model consistent with the debiased CFEPS results and complete to a limiting absolute magnitude of $H_g = 10$, a radius of $\sim$ 30 km assuming an albedo of 6%. We used the models for the classical belt populations, divided into cold, hot, and inner subpopulations, and extended the model to a minimum size of 5 km radius using the size-distribution of Fraser & Kavelaars (2009) ($q \sim 1.9$) with a break at a radius of 30 km and the ecliptic plane as the (inclination) reference plane. This resulted in a population of $\sim$ 1.9 million classical KBOs, which represents our best understanding of all the objects in stable non-resonant orbits in the Kuiper belt larger than 5 km. The Plutino population is not included.

Obtaining the perturbation-filtered proper elements by numerical orbit integration for 1.9 million test particles is too computationally expensive. Instead, we relied on the analytic secular theory of van Brouwer & van Woerkom (1950), as transcribed by Murray & Dermott (2000) to calculate proper elements for each of these bodies. We note that though this technique does not account for variations from weak mean-motion resonances (Nesvorný & Roig 2001) or higher-order secular effects, it is adequate to produce a distribution of proper elements that is consistent with the observational constraints on the Kuiper belt. Figure 1 shows the density of KBOs in the synthetic population. Here the color indicates the density of KBOs at a given point in orbital element space, with dark blue regions being empty and

[2] available online at http://www.cfeps.net/CFEPS/Suvey_Simulator.html

redder regions being more densely populated.

After obtaining the proper elements, we selected at random a KBO from the synthetic population. This KBO was then divided into a largest remnant containing half the mass and a population of smaller fragments containing the remaining mass of the original KBO. We did not perform any numerical simulations of the collisions, rather the family generation was informed by the numerical results of (Durda et al. 2007, Leinhardt & Stewart, in prep). The differential size distribution of the family was set as a power-law with index q ranging from 4-6. The minimum size cutoff of the family was set at a radius of 5 km (the same as the background synthetic population) and the density of all bodies was set to 1 g/cm^3. This choice of the cutoff size does effect the result, for $q > 4$ because most of the mass is in the smallest bodies. However, it is consistent with the location of the turnover point in the family size distribution found by Tanga et al. (1999) using a purely geometric model for the break-up of 100 km size bodies with a $M_{lr}/M_{parent} \lesssim 0.5$, as we are using here. This represents the current best constraint on family size distributions. The largest remnant was left on the same orbit as the family progenitor, unlike in the case of Levison et al. (2008b), which we do not consider to affect our overall results, while the family members were given isotropic velocity kicks with respect to the largest remnant equal to a single fixed fraction of the remnant's escape velocity. We repeated this procedure for a number of progenitor sizes and inclinations.

After inserting the synthetic collisional family into the model Kuiper belt, we calculated the minimum ejection velocity ($\Delta v_{\rm min}$) for each KBO with respect to the known collisional family largest remnant. This $\Delta v_{\rm min}$ is the minimum velocity necessary to move the potential family member from the same orbit as the largest remnant to its current orbit, allowing for any orbital orientation. It is a useful measure of the dynamical proximity between the two KBOs and is the same method originated by Ragozzine & Brown (2007) to help identify potential members of the Haumea collisional family. The $\Delta v_{\rm min}$ values were then inspected for signatures of the collisional family. Note that the calculated $\Delta v_{\rm min}$ may be smaller than the Δv imparted to the fragment because the $\Delta v_{\rm min}$ calculation uses only the orbital elements (a,e,i) and not the original orbital angles (ω,Ω,M), which are no longer known; indeed, the optimal orbital angles for each individual $\Delta v_{\rm min}$ calculation are used.

The first step in evaluating whether or not a collisional family is likely to be observable is simply to calculate the ratio of family members to background objects, $N_{\rm fam}/N_{\rm bg}$, with $\Delta v_{\rm min} \leq v_{\rm esc}$. If the ratio is $\ll 1$, the collisional family will not be clear upon visual inspection alone. For ratios ~ 1, the family may be identifiable by statistical methods. For ratios $\gg 1$, the family should stand out in a plot of KBO proper elements, as do many of the collisional families in the asteroid belt.

After this first step, the observability of families was determined for various arbitrary magnitude-limited surveys. The first step was to assign random orbital angles (ω,Ω,M) to each of the bodies in the extended synthetic population (the CFEPS Pre+L3 model included randomized angles). The apparent visual magnitude was then calculated assuming observation at opposition from (Trujillo & Brown 2001):

$$m_v = m_\odot - 2.5\log[pr^2] + 2.5\log(2.25\times10^{16}R^2(R-1)^2), \quad (5)$$

where $m_\odot = -26.75$ is the apparent V magnitude of the sun, p the albedo (assumed to be 6% for all bodies), r the radius of the body, and R the heliocentric distance. Bodies were then kept only if m_v was brighter than the magnitude cutoff.

5. Results

We inserted collisional families into the synthetic population described in Section 4 around seven different sized progenitors, ranging from 100-500 km in radius. At each size, parent bodies were selected at inclinations within 10% of 1°, 5°, 10°, 15°, and 20°. The number of family members with $r \geq 5$ km ranged from ∼1000 for 100 km bodies to ∼120000 for 500 km bodies. The fragments were given a single isotropic velocity kick relative to the largest remnant of $kv_{\rm esc}$ for $k = 0.25, 0.5, 1$. We consider this simplified case to be useful in determining what type of spread in velocities would be necessary for a collisional family to be observable. True families have members with a range of velocities relative to the center of mass, with a predicted typical $k = 1$. Although a family with k=0.25 may seem highly implausible, we need look no further than the Haumea family to see that such exotic collisional families may exist.

In this section, we first present the results for a "base case," a family that is potentially observable and has a ratio $N_{fam}/N_{bg} \sim 1$ within the orbital element volume defined by $\Delta v_{\rm min} \leq v_{\rm esc}$. We then describe the changes to the family-to-background ratio as different parameters are varied.

5.1. Base Case: A Large Progenitor in the Hot Classical Belt

Using the criteria of the ratio of family members to background objects close to the largest remnant for whether or not a family is readily identifiable, it is clear that families like those in the asteroid belt, with most of the mass having $\Delta v \sim v_{\rm esc}$, will be very difficult to identify around families with progenitors in the size (radius) range 100-500 km. Figure 2 (panels 1 and 2) shows a histogram and a cumulative number plot versus log $\Delta v_{\rm min}$ for one of

the few families with k=1 that had a family member to background KBO ratio greater than one anywhere in the orbital element volume defined by $\Delta v_{\rm min} \leq v_{\rm esc}$ and up to any limiting magnitude. Note that this family occurs in the hot classical belt at very high inclination (32°) with a progenitor of radius 470 km. As discussed in Section 3.1, it is unlikely that such a large KBO has undergone a potentially family-forming collision in the age of the solar system ($p \sim 4 \times 10^{-3}$), unless the collision probability has been greatly enhanced by the presence of scattered disk objects (Levison et al. 2008b, Section 3.2).

Figure 2 (panels 3 and 4) shows a plot of the density of KBOs in proper orbital element space. This plot includes both the background synthetic KBO population (Figure 1) and the "base case" collisional family. The family stands out visually throughout much of the classical belt region, particularly in inclinations.

5.2. Effect of Magnitude Limit

Figure 2 includes the ratio of family members to background objects at all sizes. However, the size distribution for collisional families has a larger slope than the background KBO population below the break in the size distribution, so the degree to which family members outnumber background objects will depend on size. Figure 3 (panels 1 and 2) shows histograms and cumulative number distributions versus log $\Delta v_{\rm min}$ for the same family shown in Figure 2, now including only bodies with $m_v \leq 28$. The magnitude dependence of the observability of the family is clear; the family members are outnumbered by the background objects by a factor of nearly ten. The issue is greater at even brighter magnitude limits. Panels 3 and 4 of Figure 3 again show this family plotted against the background in density, but with a magnitude limit of $m_v \leq 28$. Note that clumping of the family members is still clear to the eye in inclination-semi-major axis space.

The change in the ratio of family members to background objects within some dynamical volume given by $\Delta v_{\rm min} \leq v_{\rm esc}$ with a change in magnitude cutoff can be estimated given the size distributions of the family and the background. Given the ratio at some fixed $m_v = m_1$, the ratio at m_2 is

$$\frac{N_{fam}}{N_{bg}}|_{m_v=m_2} = \frac{N_{fam}}{N_{bg}}|_{m_v=m_1} \times 10^{(\alpha_{fam}-\alpha_{bg})(m_2-m_1)}, \quad (6)$$

where α =(q-1)/5. Thus, for a family with the same size distribution as the background, the ratio is independent of limiting magnitude. However, the ratio decreases by a factor of 100 with a change in limiting magnitude from 28 to 24.5 (the expected limiting magnitude of single exposures by LSST) if $q_{fam} \sim 4.5$ and $q_{bg} \sim 2$, as is expected below the break at $\sim$ 50 km in radius.

5.3. Effect of Location in the Belt

Figures 4 and 5 (panels 1 and 2) show histograms and cumulative number distributions versus log $\Delta v_{\rm min}$ for families with nearly identical progenitors to that of Figure 2 but located in different regions of the belt. In both Figure 4 ($\sim$ 490 km progenitor, $i \sim 2.5°$) and Figure 5 ($\sim$ 500 km progenitor, $i \sim 15°$) the family members are dominated in number by the background even at small $\Delta v_{\rm min}$ values even when no magnitude limit is included. A plot of the KBO number density including the family is shown for both Figures 4 and 5 in panels 3 and 4. The central region of the family in the cold classical belt does not stand out above the background, although some over-density does stand out at semi-major axes interior to the cold classical region, particularly in the inclinations. This region of low inclination interior to the cold classical region, is, however, unstable due to secular evolution. Note that, as discussed in Section (3.1), it is unlikely that a $\sim$ 490 km KBO would be strongly disrupted in the cold classical region anyway because of the low velocity dispersion. The effect of progenitor inclination on family identifiability will be discussed further in Section 5.9.

5.4. Effect of Progenitor Size

Figures 6 and 7 show collisional families in the hot classical belt with progenitors of size 250 km and 140 km, respectively. Although the dynamical volume $\Delta v_{\rm min} \leq v_{\rm esc}$ is much smaller for these families, the small size of the fragments and the relatively small number of fragments makes these families blend into the background population. With all else being equal, decreasing the size of the progenitor by a factor of two decreases the ratio of family members to background objects in the volume $\Delta v_{\rm min} \lesssim v_{\rm esc}$ by a factor of $\sim 2-3$. While these families will be difficult to identify using only dynamical clustering, they are by far the most likely to be present in the Kuiper belt given the strong size dependence of the collision probability. As discussed in Section 3.1, 250 km is close to the maximum size at which we would expect that there has most likely been at least one collision in the last several billion years given the current population densities. Note that the slight over-densities caused by the family are apparent to the naked eye in inclinations (panel 4) of both figures. This shows that $N_{fam}/N_{bg} \geq 1$ is not a requirement for family identification. The effect of progenitor size on family identifiability will be discussed further in Section 5.9.

5.5. Effect of Magnitude of the Velocity Dispersion

When the collisional family members are more tightly clustered, with all members having $\Delta v \leq 0.25 v_{\rm esc}$, the situation improves greatly. Such a tightly clustered family – analogous to the Haumea collisional family in orbital distribution, but still with a size distribution consistent with a catastrophic disruption event – results in family member to background object number ratios greater than one for sizes throughout the range 100-500 km. However, the inclinations at which this occurs are still $\geq 10°$. It is not entirely clear how a family would form with a considerable fraction of the mass within $\Delta v \lesssim 0.25 v_{\rm esc}$, but the existence of one such family in the Kuiper belt already makes it worth considering. Note, also, that equipartition of momentum (not necessarily an outcome of these collisions) would imply that the largest (and brightest) objects would be generally more tightly clustered.

Figure 8 (panels 1 and 2) shows a histogram and cumulative number distributions versus $\log \Delta v_{\rm min}$ for a family originating from the same progenitor as that in Figure 6, but with a typical ejection velocity of only $0.25 v_{\rm esc}$. The family members dominate in number over the background population much more so than when the relative velocities are $\sim v_{\rm esc}$. Panels 3 and 4 of Figure 8 show the tight clustering in orbital elements of the family, which stands out easily above the background. In general, decreasing the typical ejection velocity from $v_{\rm esc}$ to $0.5 v_{\rm esc}$ increases the ratio N_{fam}/N_{bg} by a factor of ~ 5. Further decreasing the typical ejection velocity to $0.25 v_{\rm esc}$, increases this ratio by another factor of ~ 5, suggesting a dependence of roughly $k^{2.5}$.

5.6. Identifying versus Characterizing Families

Thus far in this paper, we have been using the criterion that $N_{fam}/N_{bg} \geq 1$ is necessary for a family to be identifiable. However, this is not strictly true. Where the background population is well-understood, a family can be identified even when this criterion is not met. Consider a smooth background that can be accurately modeled in a particular region. In this region, the background can be subtracted from the distribution of observed KBOs. In the absence of families, the minimum fluctuations in the remaining population should be due to Poisson noise and have magnitude $\sim \sqrt{N_{bg}}$. It is now clear that families should be identifiable not only if $N_{fam} \gtrsim N_{bg}$, but also if $N_{fam} \geq \sqrt{N_{bg}}$, provided the background distribution can be well modeled and there are no "systematic" effects. In reality, there will be "systematic" effects such as clustering created by dynamical sculpting but unrelated to collisions, as in Neptune mean motion resonances. The importance of these effects will depend greatly on the location in the belt and size of the family being considered. We consider this best case to point out that it is extremely difficult or impossible to find a

family where $N_{fam} \lesssim \sqrt{N_{bg}}$.

This additional constraint now leaves us with three regimes into which a family's detectability may fall: (1) for $N_{fam} \gtrsim N_{bg}$, the family can be identified and characterized – family members can be distinguished from interlopers with some confidence, (2) for $\sqrt{N_{bg}} \leq N_{fam} < N_{bg}$, the family may be identified in the form of over-densities above the expected noise level in the background population in the absence of confounding systematics, and (3) for $N_{fam} < \sqrt{N_{bg}}$, the family cannot be identified by dynamical clustering alone.

Figure 9 shows a histogram and cumulative number distribution for the "base case" collisional family of Section 5.1, but now with the noise level ($\sqrt{N_{bg}}$) shown for the background population. It is clear that this family that had previously been deemed only marginally identifiable would stand out well above the background population, provided the background was well-behaved.

While the existence of such families can be proven by the statistically significant over-density, unless the number of family members approaches the number of background objects, it is not possible to determine which objects in the over-density belong to the family and which are interlopers without additional information. The larger the value of N_{fam}/N_{bg}, the more confidence that can be placed in the identification of individual objects as members of the family. Simple identification of families is useful, since even the number of families can help constrain the collision history of the Kuiper belt. However, insights into the properties of collisions, interiors, and surfaces requires distinguishing family members from interlopers, so there is also a clear desire to characterize families, where possible.

5.7. Using Family Shapes

Another significant increase in detectability can come by using our understanding of the shapes of families in proper element space. All calculations of $\Delta v_{\rm min}$ presented here have been using the optimal orbital angles for each object individually as suggested by Ragozzine & Brown (2007). By fixing the orbital angles (ω and f; Ω does not affect family shape) to the angle of the largest remnant, the ratio N_{fam}/N_{bg} with $\Delta v \leq v_{\rm esc}$ can be increased; the number of background objects with small Δv at a *specific* set of orbital angles drops off rapidly.

In these simulations, we are using the unrealistic assumption that all family members are launched from the parent body with $\Delta v = v_{\rm esc}$. In this case, the family lies along a 2-dimensional manifold in $a - e - i$ space that is approximately an ellipsoid in osculating elements (as in the figures of Brown et al. 2007; Ragozzine & Brown 2007, , where this

distribution is called the collisional "cloud"). If the shape of this ellipsoid were preserved in the transformation to proper elements, then using the optimal orbital angles as described above would recover nearly all of the family members in a single Δv bin. In families that cover a large range of semi-major axes, the change in secular frequencies as a function of a causes significant distortion of this ellipsoid, so that specifying the orbital angles only results in an improvement of N_{fam}/N_{bg} by an additional factor of ~ 5. It is possible to imagine attempting a search for distorted ellipsoids by scanning over the plausible set of secular frequencies in the Kuiper belt. This would effectively allow a family searching algorithm to zero in on the "arcs" visible in the distributions seen in the figures, allowing for the identification and/or characterization of families even where our metric of N_{fam}/N_{bg} and $N_{fam}/\sqrt{N_{bg}}$ would suggest a difficult to detect family. However, the improvement would be reduced in real families that have a relatively wide range of Δv values instead of the single value we have used here.

5.8. Including Color Information

The currently operating Pan-STARRS and planned LSST surveys promise to provide uniformly measured colors for a large sample of KBOs. Identification of KBO families using purely dynamical means is attractive because the physical origin of KBO colors is currently unknown and dynamical techniques allow for unbiased searches for family members. Nevertheless, the addition of color information is likely to significantly enhance family identification in the Kuiper belt. Spectral similarities were essential to the discovery of the Haumea collisional family (Brown et al. 2007). In the asteroid belt, families exhibit smaller spreads in colors than the spread in colors averaged over the entire belt (Ivezić et al. 2002; Parker et al. 2008). Identification techniques that include color information should therefore be developed.

The degree to which color information can enhance family identification depends on the mean color, μ_{fam}, and color dispersion, σ_{fam}, within a family and on the overall mean color, μ_{bg}, and color dispersion, σ_{bg}, in the family's region of the belt. Collisions may produce colors that are disjoint from the background color distribution, such that $\mu_{fam} \pm \sigma_{fam}$ and $\mu_{bg} \pm \sigma_{bg}$ do not overlap, allowing easy identification of family members using colors. We now estimate the extent to which colors enhance identification in the opposite extreme in which the two color distributions entirely overlap. We consider a family with N_{fam} members within an orbital element volume defined by $\Delta v_{min} \leq v_{esc}$ containing N_{bg} background members, as above. Considering only this dynamically-defined population, a family may be found and its members identified if $N_{fam} \gtrsim f N_{bg}$, where $f \equiv \sigma_{fam}/\sigma_{bg} \leq 1$.

Assuming that the background color distribution is well characterized, the presence of a family may be determined if $fN_{bg} \gtrsim N_{fam} \gtrsim \sqrt{fN_{bg}}+G(N_{bg})$, though in this case individual family members will not be identifiable without additional information. The factor $G(N_{bg})$ quantifies both uncertainties in the background color distribution and intrinsic variation within that distribution, which is currently unmeasured. The factor f may be viewed as an enhancement factor for both family identification and characterization and, in general, is the fraction of background objects that cannot be distinguished from family members (e.g., by colors).

The value of f is not available for as yet undetected families in the Kuiper belt, but we can look to asteroid belt families and the Haumea family for guidance. Values of the spread in $i-z$ and a^* colors from Parker et al. (2008) suggest $f = 0.1 - 0.5$ for asteroid belt families, with $i-z$ generating lower numbers than a^*. The standard deviation in B-R measured for Haumea family members compiled by Snodgrass et al. (2010) is ≈ 0.06 about a mean of $\approx$1.06. Peixinho et al. (2008) find that B-R colors in the Kuiper belt may be fit with two components: 1.71 ± 0.11 for objects with inclination $i \lesssim 12^\circ$ and 1.33 ± 0.2 for $i \gtrsim 12^\circ$. If we ignore the offset in the mean, which significantly eased the identification of the Haumea family, and only consider the dispersion, we may estimate $f \sim 0.5$ for the cold classical belt and $f \sim 0.25$ for the hot population. Fortunately, family searches do not require prior knowledge of the value of f. Choosing a value of $f = 0.25$, we estimate that color information will likely reduce the number of family members required to find and characterize a family by a factor of 4 and reduce the number required to separate the presence of a family from the statistical noise by a factor of 2. Lower values of f and the possibility that the mean color of a family may be offset from the background distribution make color measurements even more valuable. Pan-STARRS and LSST are expected to produce uniformly measured, 0.01–0.1 magnitude photometry for KBOs, precise enough to exploit color differences in family searches.

5.9. Summary

The effects of size and location of the progenitor are shown again in Figure 10. The two panels show the ratio of family members to background objects, $N_{\rm fam}/N_{\rm bg}$, versus (a) size of the progenitor and (b) inclination of the progenitor, with a magnitude limit of $m_v \leq 28$. The ratio is strongly correlated with both size and inclination, with the family "enhancement" increasing with both size and inclination of the progenitor. Thus, the easiest families to identify would be those with large progenitors at high inclinations.

The inclination dependence comes from the drop-off in background objects with in-

creasing inclination. The size dependence comes from two factors, the number of family members and the number of background objects contained within the volume $\Delta v_{\rm min} \lesssim v_{\rm esc}$. For $dN/ds \sim s^{-q_{fam}}$, with $q_{fam} > 4$, the mass is concentrated at size s_{min}. With half the mass in the largest remnant of size $R/2^{1/3}$, the number of family members at cutoff size s_{min} scales with R as

$$\frac{dN_{fam}}{ds} s|_{s_{min}} \sim \frac{\frac{1}{2}\frac{4}{3}\pi R^3 \rho}{\frac{4}{3}\pi s_{min}^3} \sim (\frac{R}{s_{min}})^3. \tag{7}$$

The number of background objects scales as

$$N_{bg} \sim \delta v^2 \sim \sqrt{\frac{M}{R}}^2 \sim R^2. \tag{8}$$

Thus, the ratio $N_{fam}/N_{bg} \sim R$ (as in Figure 10). The full size dependence, including the normalization, for the cold classical belt objects in Figure 10 is given by $N_{fam}/N_{bg} \sim 4\times10^{-5}(R/1\ {\rm km})$. For hot classical belt objects, this dependence is $N_{fam}/N_{bg} \sim 2\times10^{-4}(R/1$ km). This difference in the normalization, a factor of ~ 5, comes from the different number densities of the background population in the hot and cold classical belt regions. In Figure 10(b), the mean value of N_{fam}/N_{bg} is also a factor of ~ 5 higher in the hot belt than the cold belt (at a given size) because of the lower background density. These ratios are for a limiting magnitude $m_v = 28$ and for a typical ejection velocity of $v_{\rm esc}$, but can be scaled to any magnitude limit with Equation 6 and estimated for tighter clusterings using the results of Section 5.5.

Figure 11 shows the ratio $N_{\rm fam}/\sqrt{N_{\rm bg}}$ versus (a) size of the progenitor and (b) inclination of the progenitor. This figure shows that families could be identifiable (but not necessarily characterizable) down to sizes of $\sim$ 100 km and that the family number increasingly dominates over Poisson noise with increasing inclination.

6. Discussion

Combining a simplified understanding of the nature of collisional families from known families and numerical simulations with our present understanding of the orbital structure of the Kuiper belt, we have explored the likelihood of identifying further collisional families in the Kuiper belt if they were to exist. Given the present number of KBOs and the relative velocities in the belt, the probability that *at least one* KBO of size $\gtrsim$ 200 km has experienced a catastrophic collision in the last several billion years is close to 1. Identifying the family formed by such a collision is considerably more difficult in the Kuiper belt than in the asteroid belt due to the large region of the Kuiper belt across which the family will be

spread. A velocity dispersion of just a few hundred meters per second results in a family that is distributed across much of the classical belt region (e.g., Figure 2).

In the cold classical belt, the low relative velocities work against finding collisional families for two reasons: families are unlikely to form because large bodies will not be strongly disrupted by collisions and the clumping of the families in proper elements will not stand out against the background. Both of these problems lessen at higher inclinations, where collisional families will likely be identifiable with progenitors larger than $\sim$ 200 km. However, even at such large sizes and at high inclinations, the number of family members close to the largest remnant is still slightly lower than the number of background objects. Thus, some statistical tests relying on a sound knowledge of the background size distribution may be necessary.

It is difficult to determine a priori whether families with larger or smaller progenitors should be easier to identify. There are competing effects that influence the observability of the families: larger families have more and larger family members, while small families are more tightly clustered. In this paper, we have shown that the former effect outweighs the latter, meaning larger families should be easier to identify. For families with a steeper slope to the size distribution than the background, the larger number of family members at small sizes indicates that families will be easier to find with high magnitude limit surveys (see Equation 6), unless this signature of families is erased by subsequent collisional erosion, which is likely since most families will be nearly primordial.

Because even small ejection velocities can spread a family over large regions of the Kuiper belt, the number of family members close to the largest remnant is less than the number of "interlopers" even under most optimistic conditions. Thus, the type of clustering metric used to identify collisional families in the asteroid belt (e.g., Equation 1) and the $\Delta v_{\rm min}$ metric used to help identify potential Haumea collisional family members are not ideal for most expected Kuiper belt collisional families. The fact that family members can be dominated in number by background objects but still picked out by eye in a density map (particularly a map of inclination, see Section 5.2, Figure 3) indicates that some more suitable metric must be available.

The $\Delta v_{\rm min}$ metric can be improved somewhat by parameterizing as a function of the orbital angles (i.e., ω and f). Further improvements could be made by including color correlations into the dynamical metric. Spectral similarities were essential to the discovery of the Haumea collisional family (Brown et al. 2007). In the asteroid belt, families exhibit smaller spreads in colors than the spread in colors averaged over the entire belt (Ivezić et al. 2002; Parker et al. 2008). Though direct dynamical identification would provide a less biased detection technique for families, allowing for discovery of a broader potential range of family

constituents, identification techniques should be developed including color information.

From Figure 10, we can estimate how likely a family is to be identifiable as a function of size. Equation 4 can be inverted to calculate the number enhancement necessary for a family at a given size to have formed in the age of the solar system (or some fraction of the age of the solar system). The number of bodies of size N_t needed for a family to form with probability p is then

$$N_t = \sqrt{\frac{p}{\bar{\rho} t_l (R_i + R_t)^2} \frac{1}{10^{(q-1)\log R_t/R_i}}}, \tag{9}$$

where we have made use of the fact that $N_i = N_t \times 10^{(q-1)\log R_t/R_i}$. Thus, the number of ~ 500 km targets and ~ 350 km impactors in the classical Kuiper belt necessary for $p \sim 1$ in Equation 4 is ~ 680 and ~ 2600, respectively. This size progenitor is roughly the size necessary for solid characterization of family members, that is for $N_{fam}/N_{bg} \geq 1$ (see Figure 10).This population enhancement is a factor of ~ 16 more than the number of similar sized bodies in the Kuiper belt today. Such enhancement early in the solar system may have been possible under some formation scenarios (3.2). Identification (but not characterization) of families is possible at progenitor radii as small as ~ 200 km, where the probability of such a collision having occurred is ~ 1 without any additional enhancement.

With an improved understanding of the background population, combined with additions to the dynamical clumping metrics (e.g., colors, spectra, Δv with fixed phase angles), additional families will likely be identified by LSST.

We thank Zoe Leinhardt for helpful discussions on the nature of collisional families and for an early look at work in progress. We are also grateful to Sarah Stewart and Scott Kenyon for valuable feedback and discussion. The numerical calculations in this paper were performed on the Odyssey cluster supported by the Harvard FAS Research Computing Group.

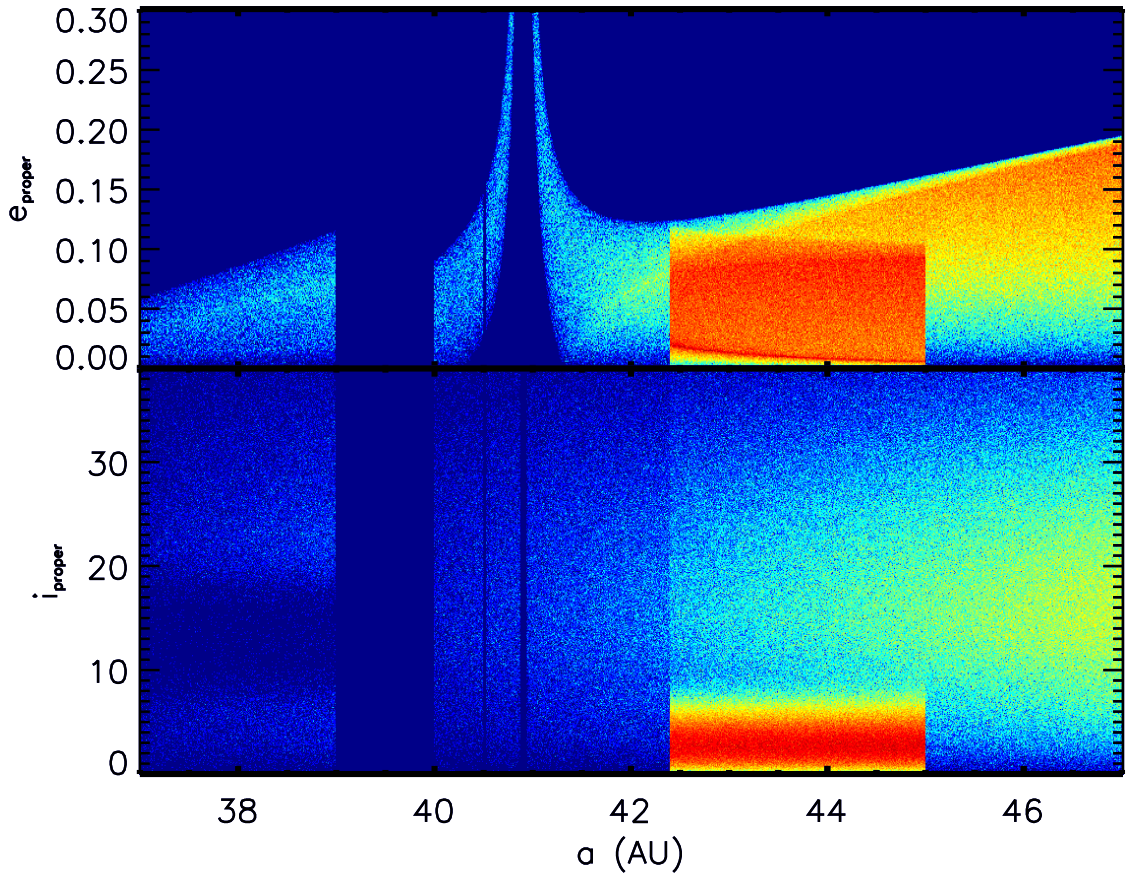

Fig. 1.— Plot of the proper orbital elements distribution of the synthetic KBO population for all bodies with no magnitude cutoff. The orbital elements were divided into 1000 bins in a, 300 bins in e_{proper}, and 400 bins in i_{proper}. The color indicates the number of bodies in the bin, with dark blue being empty, light blue containing $\sim$ 1-3, yellow indicating $\sim$ 10-20 bodies, and red corresponding to $\gtrsim$ 40 KBOs. The region near 39 AU is empty because our model contains no Plutinos (or other resonant KBOs). Vertical stripes and the upturn in eccentricities near 41 AU are due to secular resonances, which are poorly handled in our low-order secular calculation of proper elements. These minor shortcomings to the background proper element distribution do not affect our results.

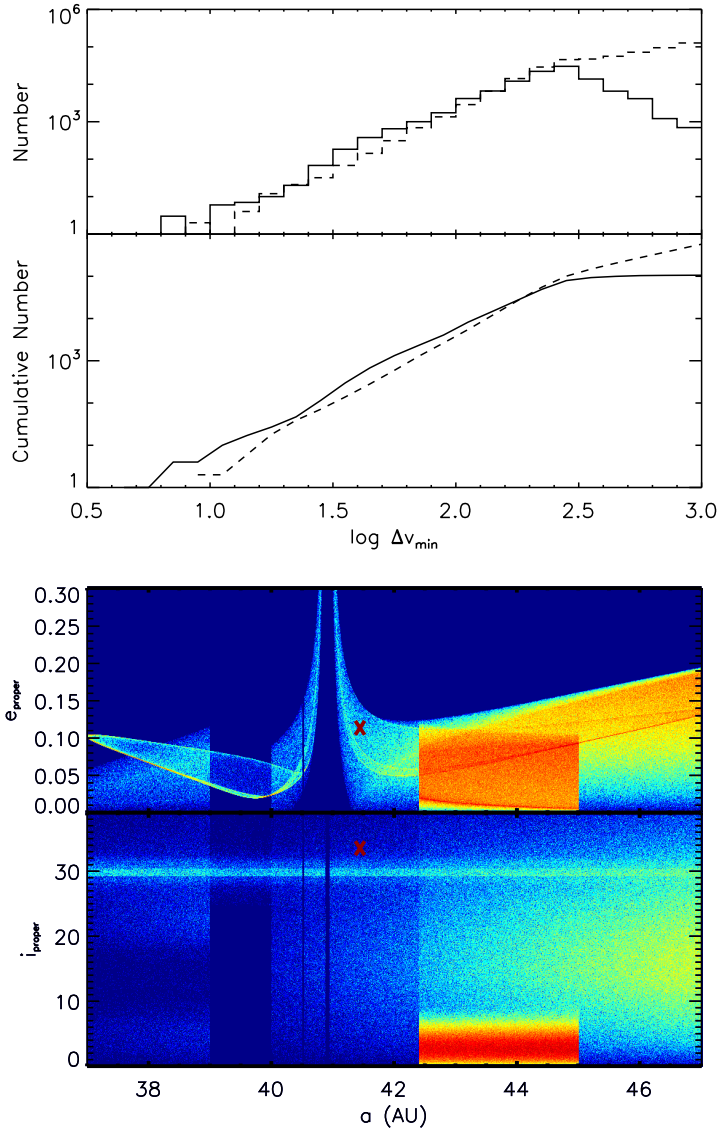

Fig. 2.— Histogram (panel 1) and cumulative number (panel 2) of KBOs versus log $\Delta v_{\rm min}$. This collisional family had a 470 km progenitor in the hot classical belt (a=41AU, e=0.1, i=32°). The family members were all given a velocity kick relative to the largest remnant of Δv=$v_{\rm esc}$. Note that the number of family members (solid line) is greater than or equal to the number of background objects (dashed line) for some values of $\Delta v_{\rm min}$. Panels 3 and 4 show the orbital element distribution of the synthetic KBO population for all bodies with no magnitude cutoff, including the collisional family. The colors are the same as in Figure 1, with redder colors indicating higher density. Note that the family stands out relative to the background particularly in inclination versus semi-major axis (bottom).

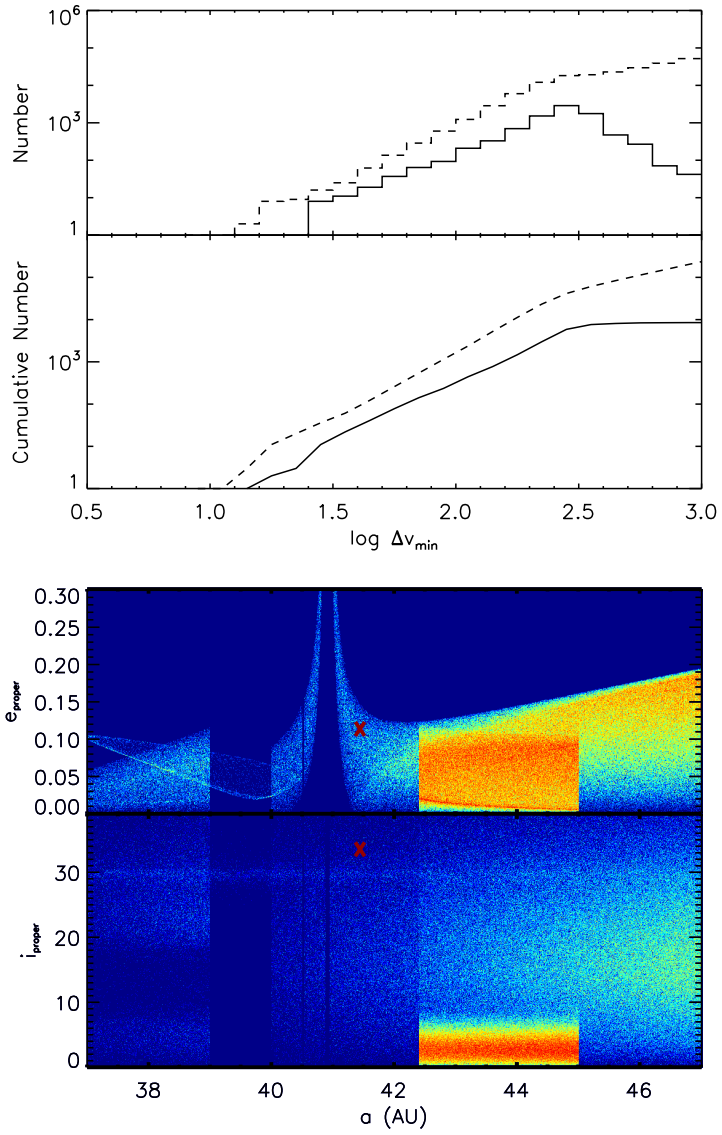

Fig. 3.— Histogram (panel 1) and cumulative number (panel 2) of KBOs with $m_v \leq 28$ versus log $\Delta v_{\rm min}$ for the same family shown in Figure 2. The family members (solid line) are now outnumbered by the background objects (dashed line) nearly ten-to-one. Panels 3 and 4 show the orbital element distribution of the synthetic KBO population for all bodies with $m_v \leq 28$, including the collisional family in Figure 2. The red 'X' indicates the location of the family's largest remnant. In this plot, yellow and red colors correspond to a factor ∼2 fewer KBOs per bin than in Figure 1. Note that the clumping of family members is still discernible to the naked eye in inclination versus semi-major axis.

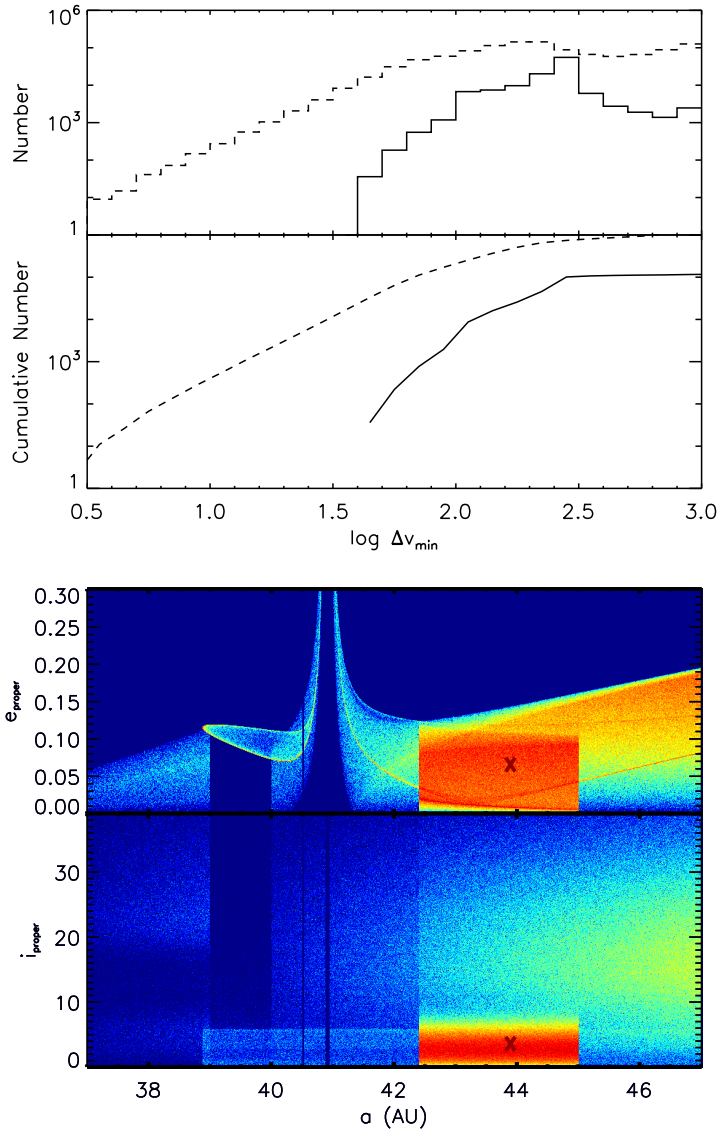

Fig. 4.— Histogram (panel 1) and cumulative number (panel 2) of KBOs versus log $\Delta v_{\rm min}$. This collisional family had a 490 km progenitor in the cold classical belt (a=44AU, e=0.06, i=2.5°). The family members were all given a velocity kick relative to the largest remnant of Δv=$v_{\rm esc}$. Note that the family members (solid line) are dominated in number by the background population (dashed line). Panels 3 and 4 show a plot of the orbital element distribution of the synthetic KBO population for all bodies with no magnitude cutoff, including the collisional family. The red 'X' indicates the location of the family's largest remnant. The colors are the same as in Figure 1. Note that the central region of the family is lost against the background population.

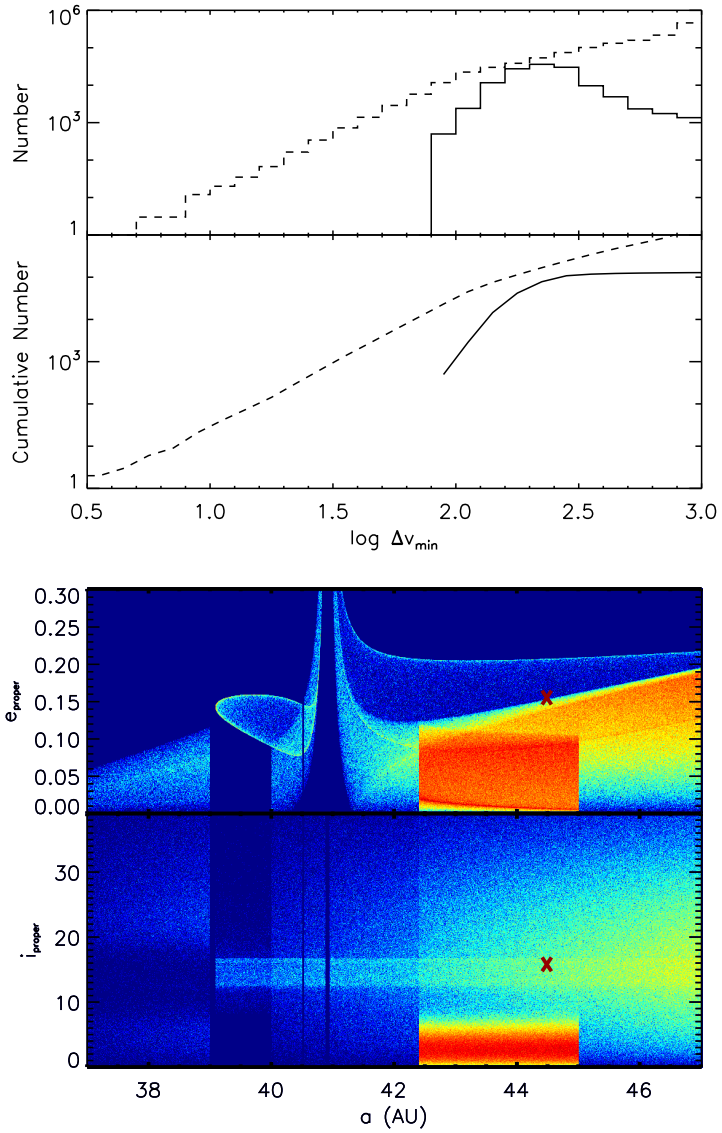

Fig. 5.— Histogram (panel 1) and cumulative number (panel 2) of KBOs versus log $\Delta v_{\rm min}$. This collisional family had a 500 km progenitor in the hot classical belt (a=44AU, e=0.15, i=15°). The family members were all given a velocity kick relative to the largest remnant of Δv=$v_{\rm esc}$. Note that the family members (solid line) are outnumbered by the background objects (dashed line) at all values of $\Delta v_{\rm min}$. Panels 3 and 4 show a plot of the orbital element distribution of the synthetic KBO population for all bodies with no magnitude cutoff, including the collisional family. The red 'X' indicates the location of the family's largest remnant. The colors are the same as in Figure 1. Note that the central region of the family is lost against the background population.

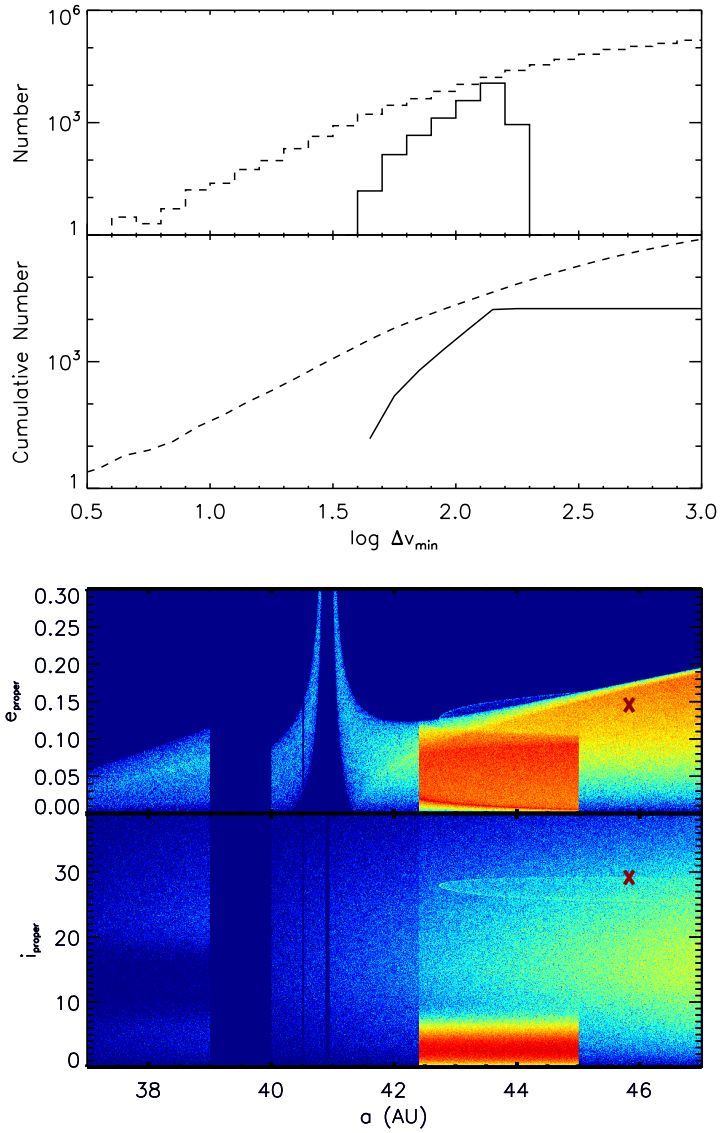

Fig. 6.— Histogram (panel 1) and cumulative number (panel 2) of KBOs versus log $\Delta v_{\rm min}$. This collisional family had a 250 km progenitor in the hot classical belt (a=46AU, e=0.14, i=28°). The family members were all given a velocity kick relative to the largest remnant of Δv=$v_{\rm esc}$. Note that the family members (solid line) are dominated in number by the background population (dashed line). Panels 3 and 4 show plots of the orbital element distribution of the synthetic KBO population for all bodies with no magnitude cutoff, including the collisional family. The red 'X' indicates the location of the family's largest remnant. The colors are the same as in Figure 1. Note that the family is clear to the naked eye in inclination versus semi-major axis.

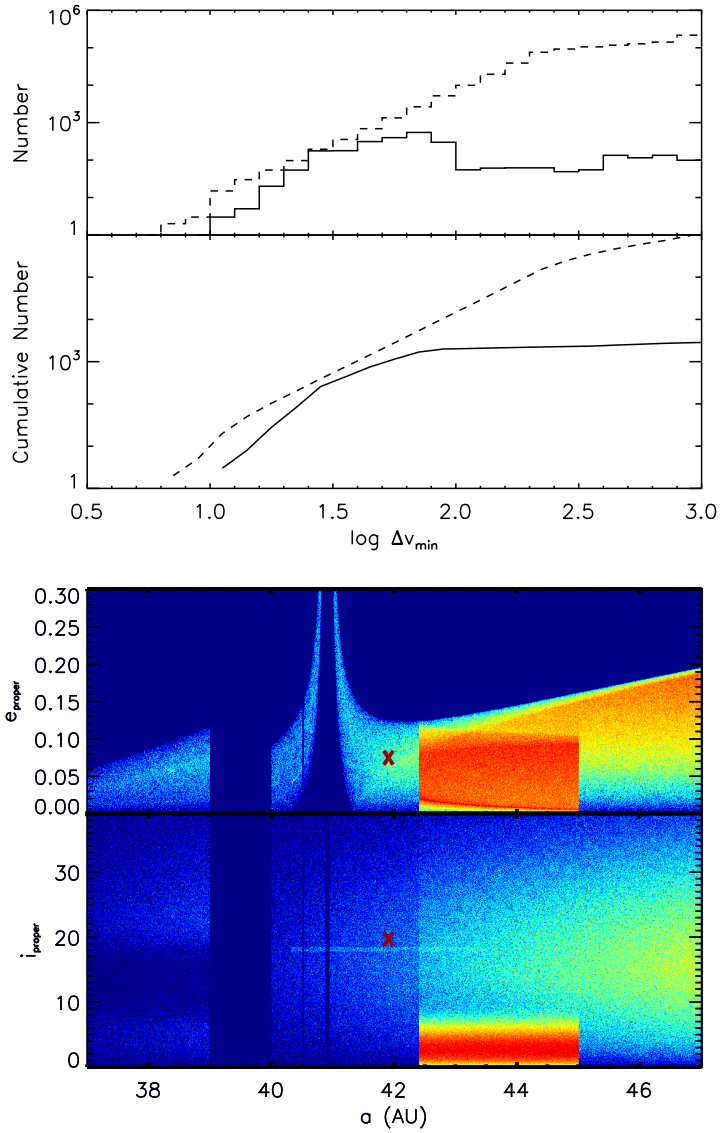

Fig. 7.— Histogram (panel 1) and cumulative number (panel 2) of KBOs versus log $\Delta v_{\rm min}$. This collisional family had a 140 km progenitor in the hot classical belt (a=42AU, e=0.07, i=19°). The family members were all given a velocity kick relative to the largest remnant of Δv=$v_{\rm esc}$. Note that the family members (solid line) are outnumbered by the background objects (dashed line) at all values of $\Delta v_{\rm min}$. Panels 3 and 4 show a plot of the orbital element distribution of the synthetic KBO population for all bodies with no magnitude cutoff, including the collisional family. The red 'X' indicates the location of the family's largest remnant. The colors are the same as in Figure 1. Note that the family is discernible to the naked eye in inclination versus semi-major axis.

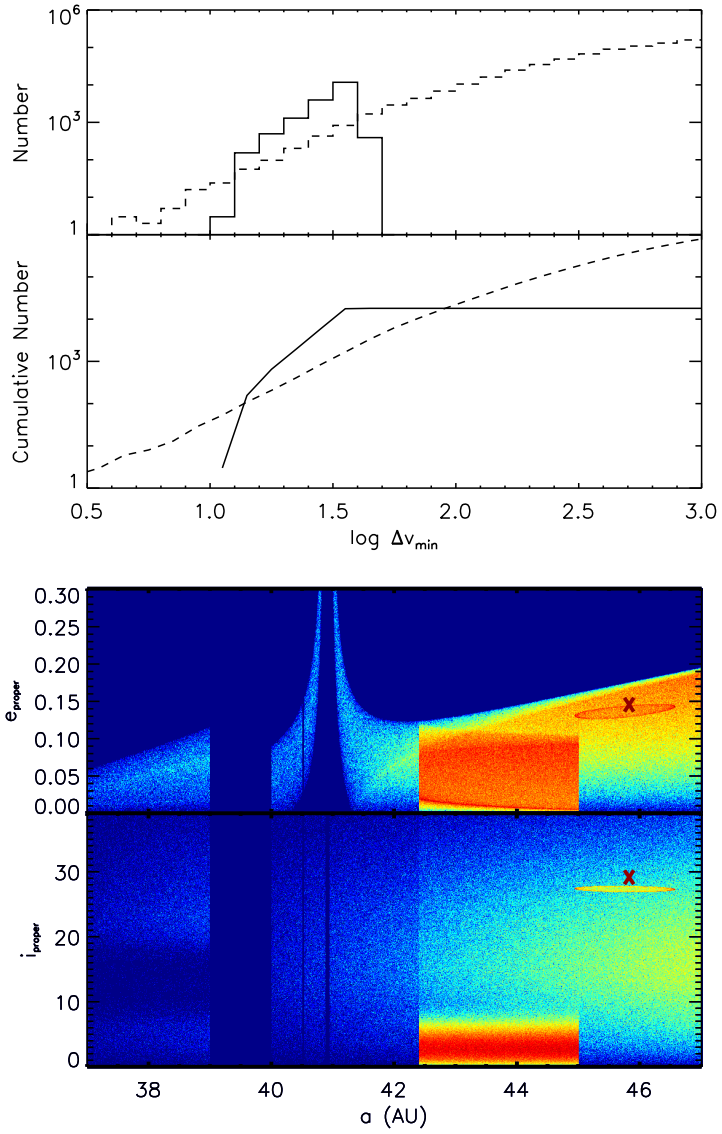

Fig. 8.— Histogram (panel 1) and cumulative number (panel 2) of KBOs versus log $\Delta v_{\rm min}$. This collisional family had the same progenitor as the family in Figure 6, a 470 km KBO in the hot classical belt (a=46AU, e=0.14, i=28°). The family members were all given a velocity kick relative to the largest remnant of Δv=0.25$v_{\rm esc}$. Note that the family members (solid line) dominate the background objects (dashed line) in number within some dynamical volume $\Delta v_{\rm min} \lesssim 2v_{\rm esc}$. Panels 3 and 4 show a plot of the orbital element distribution of the synthetic KBO population for all bodies with no magnitude limit, including the collisional family. The colors are the same as in Figure 1. Note that the family stands out relative to the background in both eccentricity versus semi-major axis and inclination versus semi-major axis.

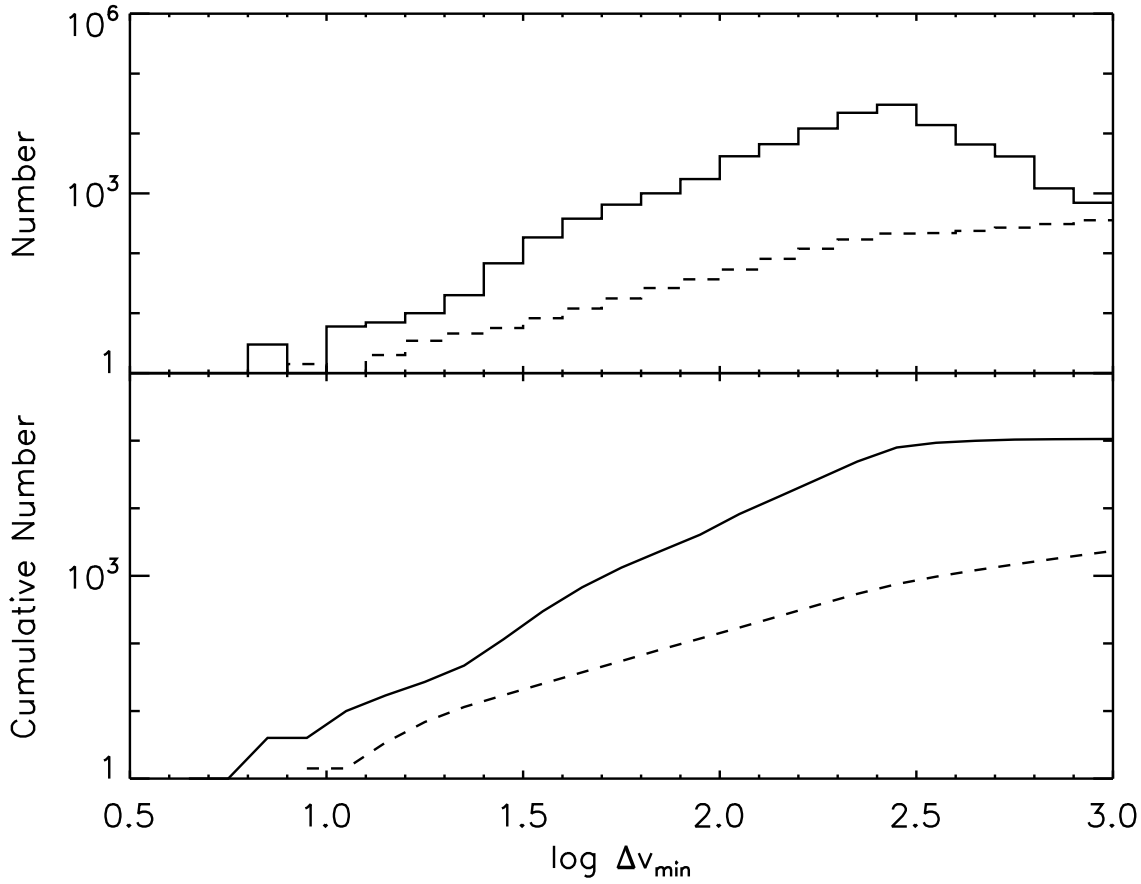

Fig. 9.— Histogram (top panel) and cumulative number (bottom panel) of KBOs versus log $\Delta v_{\rm min}$ for the "base case" collisional family (Section 5.1 and Figure 2). The family is indicated by the solid line, while the square root of the number of background objects is indicated by the dashed line. The family, which barely stood out against the background in Figure 2, clearly dominates the Poisson noise, making family identification possible by removal of the background population.

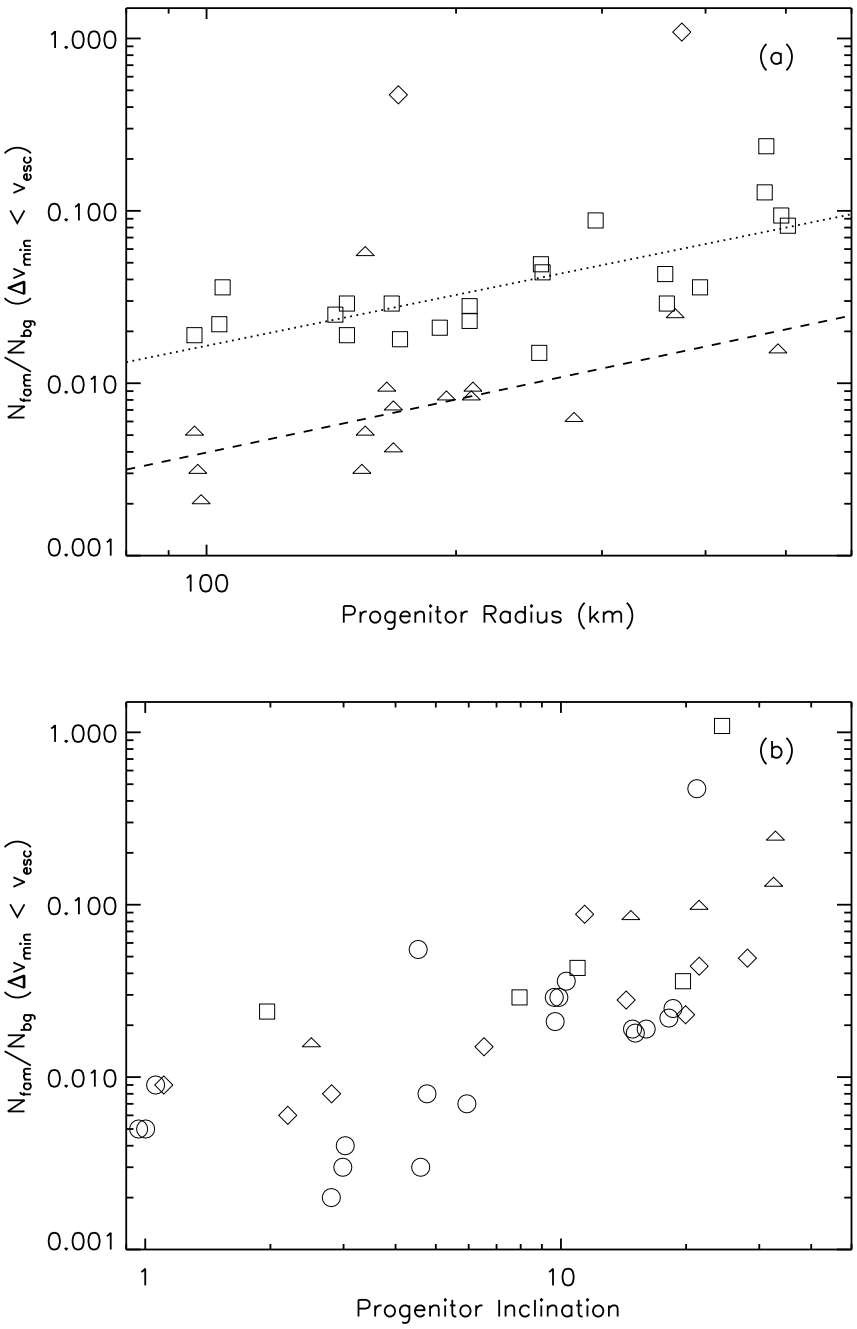

Fig. 10.— Ratio of family members to background objects with $\Delta v_{\rm min} \leq v_{\rm esc}$ versus (a) size of the progenitor and (b) inclination of the progenitor. The ratio of family members to background objects increases with both size and inclination of the progenitor. In panel (a), symbol type indicates the subpopulation to which the progenitor belonged: triangles – cold classicals, squares – hot classicals, diamonds – inner classicals. In panel (b), symbol indicates the radius of the progenitor: triangles – $R \geq 400$ km, squares – 300 km $\leq R <$ 400 km, diamonds – 200 km $\leq R <$ 300 km, circles – $R \leq 200$ km.

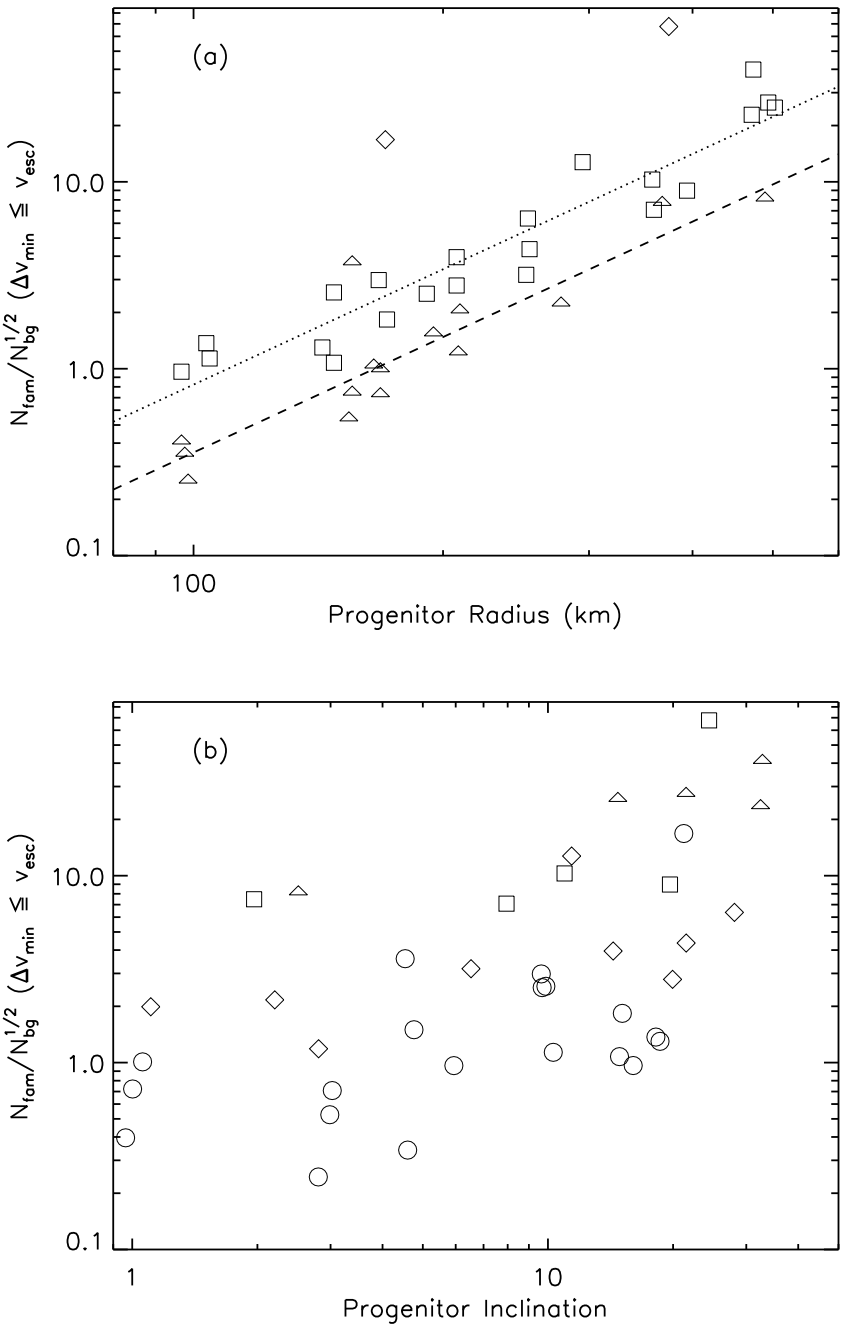

Fig. 11.— Ratio of family members, N_{fam} to the square root of the number of background objects, $\sqrt{N_{bg}}$, with $\Delta v_{\rm min} \leq v_{\rm esc}$ versus (a) size of the progenitor and (b) inclination of the progenitor. The ratio of family members to background objects increases with both size and inclination of the progenitor. In panel (a), symbol type indicates the subpopulation to which the progenitor belonged: triangles – cold classicals, squares – hot classicals, diamonds – inner classicals. In panel (b), symbol indicates the radius of the progenitor: triangles – $R \geq 400$ km, squares – 300 km $\leq R <$ 400 km, diamonds – 200 km $\leq R <$ 300 km, circles – $R \leq 200$ km.

REFERENCES

Barkume, K. M., Brown, M. E., & Schaller, E. L. 2008, AJ, 135, 55

Benecchi, S. D., Noll, K. S., Grundy, W. M., Buie, M. W., Stephens, D. C., & Levison, H. F. 2009, Icarus, 200, 292

Bernstein, G. M., Trilling, D. E., Allen, R. L., Brown, M. E., Holman, M., & Malhotra, R. 2004, AJ, 128, 1364

Bottke, Jr., W. F., Vokrouhlický, D., Rubincam, D. P., & Broz, M. 2002, Asteroids III, 395

Bottke, Jr., W. F., Vokrouhlický, D., Rubincam, D. P., & Nesvorný, D. 2006, Annual Review of Earth and Planetary Sciences, 34, 157

Brož, M., & Vokrouhlický, D. 2008, MNRAS, 390, 715

Brown, M. E. 2001, AJ, 121, 2804

Brown, M. E., Barkume, K. M., Ragozzine, D., & Schaller, E. L. 2007, Nature, 446, 294

Brucker, M. J., Grundy, W. M., Stansberry, J. A., Spencer, J. R., Sheppard, S. S., Chiang, E. I., & Buie, M. W. 2009, Icarus, 201, 284

Cellino, A., & Dell'Oro, A. 2010, in Lecture Notes in Physics, Berlin Springer Verlag, Vol. 790, Lecture Notes in Physics, Berlin Springer Verlag, ed. J. Souchay, 137–193

Chiang, E., Lithwick, Y., Murray-Clay, R., Buie, M., Grundy, W., & Holman, M. 2007, Protostars and Planets V, 895

Chiang, E. I. 2002, ApJ, 573, L65

Chiang, E. I., Lovering, J. R., Millis, R. L., Buie, M. W., Wasserman, L. H., & Meech, K. J. 2003, Earth Moon and Planets, 92, 49

Davis, D. R., & Farinella, P. 1996, in Lunar and Planetary Institute Science Conference Abstracts, Vol. 27, Lunar and Planetary Institute Science Conference Abstracts, 293–+

Durda, D. D., Bottke, W. F., Nesvorný, D., Enke, B. L., Merline, W. J., Asphaug, E., & Richardson, D. C. 2007, Icarus, 186, 498

Elliot, J. L., et al. 2005, AJ, 129, 1117

—. 2010, Nature, 465, 897

Fraser, W. C., Brown, M. E., & Schwamb, M. E. 2010, ArXiv e-prints

Fraser, W. C., & Kavelaars, J. J. 2009, AJ, 137, 72

Fuentes, C. I., George, M. R., & Holman, M. J. 2009, ApJ, 696, 91

Fuentes, C. I., Holman, M. J., Trilling, D. E., & Protopapas, P. 2010, ArXiv e-prints

Gladman, B., Marsden, B. G., & Vanlaerhoven, C. 2008, Nomenclature in the Outer Solar System, ed. Barucci, M. A., Boehnhardt, H., Cruikshank, D. P., & Morbidelli, A. , 43–57

Gomes, R., Levison, H. F., Tsiganis, K., & Morbidelli, A. 2005, Nature, 435, 466

Hahn, J. M., & Ward, W. R. 1995, in Lunar and Planetary Inst. Technical Report, Vol. 26, Lunar and Planetary Institute Science Conference Abstracts, 541–+

Hirayama, K. 1918, AJ, 31, 185

Ivezić, Ž., et al. 2002, AJ, 124, 2943

Kavelaars, J. J., et al. 2009, AJ, 137, 4917

Kenyon, S. J., Bromley, B. C., O'Brien, D. P., & Davis, D. R. 2008, Formation and Collisional Evolution of Kuiper Belt Objects, ed. Barucci, M. A., Boehnhardt, H., Cruikshank, D. P., & Morbidelli, A. , 293–313

Knežević, Z., & Milani, A. 2000, Celestial Mechanics and Dynamical Astronomy, 78, 17

Leinhardt, Z. M., Marcus, R. A., & Stewart, S. T. 2010, ApJ, 714, 1789

Levison, H. F., Morbidelli, A., Vanlaerhoven, C., Gomes, R., & Tsiganis, K. 2008a, Icarus, 196, 258

Levison, H. F., Morbidelli, A., Vokrouhlický, D., & Bottke, W. F. 2008b, AJ, 136, 1079

Levison, H. F., & Stern, S. A. 2001, AJ, 121, 1730

Lykawka, P. S., & Mukai, T. 2007, Icarus, 192, 238

Malhotra, R. 1995, AJ, 110, 420

Milani, A. 1993, Celestial Mechanics and Dynamical Astronomy, 57, 59

Milani, A., & Farinella, P. 1994, Nature, 370, 40

Morbidelli, A., Levison, H. F., & Gomes, R. 2008, The Dynamical Structure of the Kuiper Belt and Its Primordial Origin, ed. Barucci, M. A., Boehnhardt, H., Cruikshank, D. P., & Morbidelli, A. , 275–292

Murray, C. D., & Dermott, S. F. 2000, Solar System Dynamics, ed. Murray, C. D. & Dermott, S. F.

Nesvorný, D., Bottke, Jr., W. F., Dones, L., & Levison, H. F. 2002, Nature, 417, 720

Nesvorný, D., & Roig, F. 2001, Icarus, 150, 104

Noll, K. S., Grundy, W. M., Stephens, D. C., Levison, H. F., & Kern, S. D. 2008, Icarus, 194, 758

Pan, M., & Sari, R. 2005, Icarus, 173, 342

Parker, A., Ivezić, Ž., Jurić, M., Lupton, R., Sekora, M. D., & Kowalski, A. 2008, Icarus, 198, 138

Peixinho, N., Lacerda, P., & Jewitt, D. 2008, AJ, 136, 1837

Petit, J., & Mousis, O. 2004, Icarus, 168, 409

Pitjeva, E. V. 2010, in IAU Symposium, Vol. 263, IAU Symposium, ed. J. A. Fernández, D. Lazzaro, D. Prialnik, & R. Schulz , 93–97

Pravec, P., et al. 2010, Nature, 466, 1085

Rabinowitz, D. L., Schaefer, B. E., Schaefer, M., & Tourtellotte, S. W. 2008, AJ, 136, 1502

Ragozzine, D., & Brown, M. E. 2007, AJ, 134, 2160

Schlichting, H. E., Ofek, E. O., Wenz, M., Sari, R., Gal-Yam, A., Livio, M., Nelan, E., & Zucker, S. 2009, Nature, 462, 895

Schlichting, H. E., & Sari, R. 2008, ApJ, 686, 741

—. 2009, ApJ, 700, 1242

Sheppard, S. S. 2010, AJ, 139, 1394

Snodgrass, C., Carry, B., Dumas, C., & Hainaut, O. 2010, A&A, 511, A72+

Stewart, S. T., & Leinhardt, Z. M. 2009, ApJ, 691, L133

Tanga, P., Cellino, A., Michel, P., Zappalà, V., Paolicchi, P., & dell'Oro, A. 1999, Icarus, 141, 65

Toth, I., & Lisse, C. M. 2010, in IAU Symposium, Vol. 263, IAU Symposium, ed. J. A. Fernández, D. Lazzaro, D. Prialnik, & R. Schulz , 131–140

Trujillo, C. A., & Brown, M. E. 2001, ApJ, 554, L95

van Brouwer, D., & van Woerkom, A. J. J. 1950, Astronomical papers prepared for the use of the American ephemeris and nautical almanac, v.13, pt.2, Washington : U.S. Govt. Print. Off., 1950., p. 81-107 : 29 cm., 13, 81

Vernazza, P., Binzel, R. P., Rossi, A., Fulchignoni, M., & Birlan, M. 2009, Nature, 458, 993

Vokrouhlický, D. 1999, A&A, 344, 362

Vokrouhlický, D., & Nesvorný, D. 2008, AJ, 136, 280

—. 2009, AJ, 137, 111

Zappala, V., Bendjoya, P., Cellino, A., Farinella, P., & Froeschle, C. 1995, Icarus, 116, 291

Zappala, V., Cellino, A., Farinella, P., & Knezevic, Z. 1990, AJ, 100, 2030